Myeloid-mesenchymal crosstalk drives Arg1-dependent profibrotic metabolism via ornithine in lung fibrosis

Authors

Preeti Yadav[1,2], Javier Gómez Ortega[1,2], Prerna Dabral[3,4], Whitney Tamaki[5,6], Charles Chien[7,8], Kai-chun Chang[9,10], Nivedita Biswas[1,2], Sixuan Pan[10], Julia Nilsson[4], Xiaoyang Yin[1,2,11], Aritra Bhattacharyya[1,2,12], Kaveh Boostanpour[1,2], Tanay Jujaray[1,2], Jasper Wang[1,2], Tatsuya Tsukui[1,13], Chris Molina[1,13], Vincent Auyeung[1,13], Dean Sheppard[1,13], Baosheng Li[11], Mazharul Maishan[1], Hiroki Taenaka[1], Michael A. Matthay[1], Rieko Muramatsu[14], Lenka Maliskova[15], Arnab Ghosh[15], Walter L. Eckalbar[15], Ari B. Molofsky[4], Stanley J. Tamaki[15], Trever Bivona[3,4,16], Adam R. Abate[10], Allon Wagner[7,8,17], Satish K. Pillai[3,4], Paul J. Wolters[1], Kevin M. Tharp[18], Mallar Bhattacharya[1,2§]

Affiliations

[1]Division of Pulmonary, Critical Care, Allergy, and Sleep, Department of Medicine, University of California, San Francisco, San Francisco, CA, USA
[2]Sandler Asthma Basic Research Center, University of California, San Francisco, San Francisco, CA, USA
[3]Vitalant Research Institute, San Francisco, California.
[4]Department of Laboratory Medicine, University of California, San Francisco, San Francisco, California, USA.
[5]Department of Medicine, University of California, San Francisco, San Francisco, CA 94158, USA.
[6]Helen Diller Family Comprehensive Cancer Center, University of California, San Francisco, San Francisco, CA 94158, USA.
[7]Department of Electrical Engineering and Computer Sciences, University of California, Berkeley, CA 94720, USA
[8]Center for Computational Biology, University of California, Berkeley, CA 94720, USA
[9]Twist Bioscience, 681 Gateway Blvd, South San Francisco, CA, USA
[10]Department of Bioengineering and Therapeutic Sciences, University of California, San Francisco, San Francisco, CA, USA
[11]Department of Radiation Oncology, Shandong Cancer Hospital and Institute, Shandong First Medical University and Shandong Academy of Medical Sciences, Jinan, China
[12]Biological Science Division, Indian Statistical Institute, Kolkata, India.
[13]Cardiovascular Research Institute; University of California, San Francisco, San Francisco, CA, USA
[14]Department of Molecular Pharmacology, National Institute of Neuroscience, National Center of Neurology and Psychiatry, Kodaira, Japan
[15]UCSF CoLabs, University of California, San Francisco, San Francisco, CA 94143, USA
[16]Chan-Zuckerberg Biohub, San Francisco, CA 94158, USA.
[17]Department of Molecular and Cell Biology, University of California, Berkeley, CA 94720, USA
[18]Cancer Metabolism and Microenvironment Program, NCI-Designated Cancer Center, Sanford Burnham Prebys Medical Discovery Institute, La Jolla, CA, USA

§ Correspondence: Mallar Bhattacharya
Email: mallar.bhattacharya@ucsf.edu
Phone: 415-514-1018
Address: 513 Parnassus Avenue, HSE-201P, San Francisco, CA 94143, USA

Declaration of Interests

The authors have declared that no conflict of interest exists.

Abstract

Idiopathic pulmonary fibrosis (IPF) is a disease of progressive lung remodeling and collagen deposition that leads to respiratory failure. Myeloid cells are abundant in IPF lung and in murine lung fibrosis, but their functional effects are incompletely understood. Using mouse and human lung models, we show that ornithine produced by myeloid cells expressing Arg1 serves as a substrate for proline and collagen synthesis by lung fibroblasts. The predominant Arg1-expressing myeloid cells in mouse lung were macrophages, but in IPF lung, high-dimensional imaging revealed ARG1 to be expressed mainly in neutrophils. Arg1 inhibition suppressed both ornithine levels and collagen expression in cultured, precision-cut IPF lung slices and in murine lung fibrosis. These results were confirmed in macrophage-specific Arg1 KO mice. Furthermore, we find that this pathway is regulated by cell-to-cell crosstalk, starting with purinergic signaling: Fibroblast eATP receptor P2rx4 was necessary for fibroblast IL-6 expression, which in turn was necessary for Arg1 expression by myeloid cells. Taken together, our findings define an immune-mesenchymal circuit that governs profibrotic metabolism in lung fibrosis.

Keywords

Myeloid Arginase 1; Fibroblasts; Fibrosis; IPF; Ornithine

67 **Introduction**

68 Pathologic fibrosis is a destructive response to tissue injury that results from the deposition of excess
69 fibrillar collagen by activated fibroblasts. In idiopathic pulmonary fibrosis (IPF), it is believed that
70 dysfunction of the epithelium leads to the recruitment and activation of multiple cell types, including
71 most importantly fibroblasts and myeloid cells (1). These cells have been found to be in close proximity
72 in the fibrotic niche (2, 3), but it remains unclear how they interact to induce the fibrotic phenotype. One
73 approach is to define and test the functional role of diffusible factors that have been detected in fibrosis
74 and that might subserve crosstalk between the various cell types leading to collagen production by
75 fibroblasts.

76 We recently considered the role of extracellular ATP (eATP), a damage-associated molecular
77 pattern (DAMP) molecule that is extensively present in the IPF lung, as revealed in the bronchoalveolar
78 lavage from patients for example (4). eATP's role in fibrosis remains incompletely understood.
79 Although eATP activates receptor-mediated transcriptional responses by ligating multiple purinergic
80 receptors, in lung fibroblasts we reported P2rx4 as the critical purinergic receptor: Fibroblast-specific
81 deletion of the eATP receptor P2rx4 decreased lung fibrosis in mice (5). However, the paracrine
82 signaling effects of this pathway are not known.

83 Here we explore the effect of P2rx4 signaling on cell-to-cell crosstalk in fibrosis. Recent studies
84 have revealed a heterogeneity of fibroblast states following injury, and inflammatory fibroblasts have
85 been detected as a distinct subset of mesenchymal cells that express secreted inflammatory factors
86 such as chemokines and cytokines (6-8). How these signals from inflammatory fibroblasts promote
87 fibrosis is unknown. We hypothesized that eATP-P2rx4 signaling may stimulate expression of these
88 diffusible signals from fibroblasts after injury, initiating profibrotic crosstalk with other cells in the fibrotic
89 niche.

90 Studies with murine macrophage-fibroblast cocultures revealed that macrophage Arg1
91 expression was dependent on P2rx4 signaling in fibroblasts. Arg1+ macrophages were increased after
92 bleomycin-induced lung fibrosis in mice; in IPF lung, ARG1+ cells were also increased, in the neutrophil
93 compartment. In both murine and human lung systems, Arg1 inhibition decreased lung fibrosis.

94 Furthermore, Arg1 was induced by fibroblast expression of the cytokine IL-6 in a P2rx4-dependent
95 manner. Mechanistically, Arg1 drove fibroblast collagen synthesis via the production of the noncoding
96 amino acid ornithine, which served as a precursor for the collagen building block proline. These findings
97 indicate a critical profibrotic role for a metabolic pathway arising from cellular crosstalk in the
98 development of lung fibrosis.
99
100

101 **Results**

102 ***Arg1+ cells localize to the fibrotic niche.*** We recently reported that mice with deletion of the eATP
103 receptor P2rx4 in fibroblasts were protected from bleomycin injury-induced lung fibrosis (5). To screen
104 for macrophage genes regulated by fibroblast eATP-P2rx4 signaling, we used an *in vitro* system: Either
105 WT or P2rx4 KO fibroblasts were cocultured with WT lung macrophages (**Supplemental Figure 1A**),
106 followed by single cell RNAseq. Both cell types were isolated from murine lungs 7 days after injury to
107 approximate cellular states during the early fibrotic period, defined by increased fibroblast expression of
108 Col1a1 and Col3a1 (**Supplemental Figure 1B**). Fibroblasts were used directly, whereas macrophages
109 were treated for 48 hours in culture with Csf1 to maintain macrophage identity prior to coculture. After 5
110 days of coculture, cells were submitted for scRNAseq.

111 The most downregulated macrophage gene when fibroblast P2rx4 was deleted was Arg1, a
112 marker of alternatively activated macrophages (**Figure 1A**). Analysis of lung macrophages in a
113 published scRNAseq time course following bleomycin lung injury (9) showed maximal *Arg1* in the "C2",
114 transitional macrophage compartment that we previously demonstrated was localized to the fibrotic
115 niche after injury(2) (**Figure 1B**). C2 cells expressed higher levels of Arg1 and also the "Fab5" marker
116 genes that were recently found to be associated with a core pro-fibrotic macrophage program (10)
117 (**Supplemental Figure 1C-E**), and they were transcriptomically similar to recruited and interstitial
118 macrophages (11) (**Supplemental Figure 1F**). Interestingly, the macrophages from our cocultures also
119 expressed higher levels of interstitial macrophage than alveolar macrophage genes (**Supplemental**
120 **Figure 1G**). To determine whether Arg1+ cells localized to areas of fibrosis, we injured mice expressing
121 reporter alleles for Arg1 and for the fibroblast marker Col1a1. Confocal imaging revealed that Arg1+
122 cells were in proximity to clusters of activated fibroblasts in the fibrotic niche (**Figure 1C**).

123 To further profile Arg1 expression in myeloid cell subsets in mice, we performed flow cytometry
124 with Arg1 reporter mice. This analysis confirmed that Arg1 was expressed 10 days after bleomycin
125 injury in macrophages expressing CD11b and CD64, markers consistent with monocyte-derived
126 macrophages (**Supplemental Figure 2A-C**). Canonical neutrophils expressing Ly6G did not express
127 Arg1, which we confirmed by immunofluorescence for the neutrophil marker S100A8 (**Supplemental**

128 **Figure 2D**). However, we did note emergence of a small myeloid population of Arg1+ cells expressing
129 Ly6G that also expressed CD64 and CD11c, though this population was about tenfold smaller in
130 number than moMacs (**Supplemental Figure 2E**). Taken together, these data confirm expression of
131 Arg1 in myeloid cells in the mouse lung fibrotic niche.
132 To determine the relevance of ARG1 to IPF, we first interrogated a published dataset of BAL
133 cell gene expression by microarray (12). This analysis confirmed higher ARG1 expression in IPF
134 compared to healthy controls (**Figure 1D**). We then found increased ARG1+ cells by
135 immunofluorescence of IPF lung explants acquired at the time of clinical transplantation compared with
136 deceased donor lungs not known to have lung disease (**Figure 1E; Supplemental Table 1**). In human
137 lung, ARG1 has been found to be expressed in neutrophils, based on data from lung cancer specimens
138 (13-15). However, deep phenotyping in IPF lung tissue of ARG1-expressing cell types has not been
139 undertaken. Therefore, to comprehensively profile the cell types expressing ARG1 in IPF, we
140 performed multiplexed ion beam imaging (MIBI) (16-19), an antibody-based imaging technique in which
141 isotopically pure elemental metal reporters are conjugated to antibodies and detected spatially in
142 combination with mass spectrometry. We applied MIBI to sections from 5 IPF explanted lungs using
143 anti-ARG1 antibody and 33 other antibodies, selecting markers primarily for the purpose of defining
144 major immune cell types. These data showed that ARG1+ cells predominantly expressed the
145 neutrophil-specific markers CD66B and MPO but not the macrophage markers CD68, CD206, and
146 CD163 (**Figure 2A-C; Supplemental Table 2**). Importantly, neutrophils have been associated with
147 increased mortality in IPF (20-23). However, their function in fibrogenesis has not been well studied.
148
149 ***Arg1 regulates availability of ornithine, a pro-fibrotic substrate*.** To understand Arg1's function, we
150 considered first that ornithine generated from arginine by Arg1 can serve as a substrate for the
151 synthesis of proline (24), a major constituent of collagen. Remarkably, we found that ornithine was
152 markedly increased both in mouse lung 14 days after bleomycin injury compared to steady state and in
153 IPF lung lysates compared to healthy controls (**Figure 3A**). To test the effects of Arg1 and ornithine in
154 fibrosis, we first used the small-molecule Arg1 inhibitor CB-1158 (25). We confirmed the on-target effect

155 of CB-1158 by measuring lung ornithine after treatment: In both bleomycin-injured mice and precision-
156 cut lung slices (PCLS) from explanted IPF lungs, the inhibitor decreased ornithine levels (**Figure 3B**).
157 Next, we treated bleomycin-injured mice with CB-1158 during the fibrotic period. Importantly, we found
158 that lung fibrosis was significantly decreased and body weight recovery improved with Arg1 inhibition
159 (**Figure 3C; Supplemental Figure 2F**). We then prepared PCLS from explanted IPF lungs and treated
160 them with CB-1158 for 24 hours, followed by immunoblot for COL1A1 in the RIPA buffer-soluble
161 fraction representing the more soluble, newly synthesized collagen (26). COL1A1 expression measured
162 by immunoblot of lung slice lysates was decreased by CB-1158 treatment compared to untreated
163 controls, indicating suppression of collagen synthesis with ARG1 inhibition (**Figure 3D**). Retention of
164 cells expressing ARG1 and neutrophil markers MPO and CD66B was confirmed in PCLS by
165 immunofluorescence (**Supplemental Figure 3A**). Finally, taking a genetic approach with macrophage-
166 specific Arg1 KO mice in which Cre-mediated deletion efficiency was approximately 55%
167 (**Supplementary Figure 3B**), we found that lung fibrosis was significantly decreased after injury in KO
168 mice compared to controls (**Figure 3E**). Taken together, these data indicate that Arg1 determines the
169 pathologic accumulation of collagen in lung fibrosis.
170 We then tested the effect of ornithine on collagen expression. First, we found that exogenous
171 ornithine increased fibroblast collagen expression by immunofluorescence in monocultured fibroblasts
172 from both mouse and human lung (**Figure 3F**). To test the profibrotic potential of ornithine *in vivo*, we
173 treated mice with ornithine by oral gavage, either at steady state or during the fibrotic phase after
174 bleomycin injury. Ornithine treatment increased lung collagen production in the setting of injury but not
175 at steady state, consistent with increased cellular demand for collagen synthetic precursors including
176 proline during fibrogenesis (**Figure 3G**). We then found that macrophage-fibroblast coculture increased
177 collagen expression compared to fibroblast monoculture, an effect that could be blocked with CB-1158
178 or fibroblast P2rx4 KO and enhanced with ornithine (**Figure 3H-I**). Furthermore, ornithine could rescue
179 the CB-1158-dependent decreased collagen expression in cocultures (**Supplemental Figure 3C**).
180 Finally, fibroblast coculture with Arg1-specific KO macrophages was associated with decreased
181 collagen expression compared with WT macrophages, an effect that was not significantly augmented

182 with CB-1158 (**Figure 3J**). Taken together, these results indicate a direct profibrotic effect of ornithine
183 *in vitro* and *in vivo*.
184 Ornithine is converted by ornithine aminotransferase (OAT) to glutamate-5-semialdehyde, which
185 spontaneously cyclizes to pyrroline-5-carboxylate and is then reduced by P5C reductases to proline.
186 Notably, OAT inhibition decreased coculture-dependent augmentation of collagen expression
187 (**Supplemental Figure 3C**). Interestingly, coculture also increased α-SMA expression, but this effect
188 was not augmented by ornithine or suppressed by OAT inhibition (**Supplemental Figure 3D)**. These
189 data indicate a dependence of collagen synthesis on Arg1 function and ornithine metabolism. Finally,
190 we directly tested the hypothesis that Arg1-mediated ornithine production was necessary for increasing
191 fibroblast proline content, using the approach of macrophage-fibroblast coculture followed by isolation
192 of fibroblasts for LC-MS to detect proline. Consistent with our hypothesis, Arg1 inhibition with CB-1158
193 significantly decreased fibroblast proline content in cocultures (**Figure 3K**). Taken together, these
194 results suggest that macrophage Arg1 drives fibrosis by producing ornithine, which serves as a
195 substrate for fibroblast proline synthesis, augmenting collagen expression.
196
197 ***Arg1 is regulated by IL-6.*** To determine how macrophage Arg1 expression is regulated by signaling
198 within the fibrotic niche, we considered that our previously described coculture data (**Figure 1A**)
199 indicated that P2rx4 signaling in fibroblasts was necessary for Arg1 expression in cocultured
200 macrophages. Therefore, we performed analysis of ligand-receptor interactions via CellChat (27) and
201 Ingenuity Pathways Analysis. This analysis revealed suppression of IL-6 signaling in the P2rx4 KO
202 condition (**Figure 4A**). We also found that P2rx4 KO fibroblasts expressed less IL-6 mRNA compared
203 to WT (**Figure 4B**). IL-6 is an important profibrotic factor and is a therapeutic target in clinical lung
204 fibrosis (28-31). We first confirmed an increase of Arg1 in cultured mouse lung macrophages treated
205 with IL-6 (**Figure 4C**). *In vivo*, we noted that IL-6 KO mice had decreased macrophage numbers in the
206 lung, consistent with a chemotactic effect of IL-6 (**Supplemental Figure 3E**). Nonetheless, even
207 accounting for this lower cell count, Arg1 lavage levels were disproportionately decreased in IL-6 KO
208 mice, as indicated by bronchoalveolar lavage Arg1 concentrations normalized to CD11b+CD64+

209 macrophage count and by qPCR measurement of *Arg1* relative to *Gapdh* in flow-sorted CD11b+CD64+
210 macrophages (**Figure 4D**). Of note, IL-6 KO mice had decreased lung fibrosis after bleomycin lung
211 injury (**Supplemental Figure 3F**). We then analyzed scRNAseq time course data for multiple lung cell
212 types and found that IL-6 was indeed highly expressed in fibroblasts relative to other cell types (**Figure**
213 **4E**). Furthermore, IL-6 was notably expressed in the emergent, disease-associated inflammatory and
214 fibrotic fibroblasts observed in recent time course data (8) (**Figure 4F**).

215 To test whether IL-6 could induce ARG1 in human lung, we first tested PCLS from explanted
216 IPF lungs. Treatment with the IL-6R blocking antibody tocilizumab for 24 hours decreased ARG1
217 expression in IPF PCLS lysates (**Figure 5A**). To confirm that paracrine interaction between ARG1+ and
218 IL-6+ cells was spatially plausible, we analyzed spatial transcriptomic data of IPF samples. For this
219 purpose, we defined a proximity statistic that allowed us to quantitatively compare the probabilities of
220 detecting an IL6+ fibroblast versus an IL6- fibroblast, within a given distance from an ARG1+ cell
221 (**Methods**). Interestingly, at a distance from ARG1+ cells consistent with potential paracrine signaling
222 (25 microns), fibroblasts were significantly more likely to express IL-6 than not to express IL-6 (**Figure**
223 **5B**). These data are consistent with paracrine IL-6 signaling from fibroblasts to macrophages resulting
224 in ARG1 induction in IPF.

225 We then interrogated published datasets for neutrophils from lung tissue to test whether ARG1+
226 neutrophils were more likely to express IL6R and therefore to support IL6 signaling. While genome-
227 wide transcriptomic profiling of neutrophils from human fibrotic lungs has not yet been reported in the
228 literature, as an alternative, we analyzed aggregate data from available non-small cell lung cancer
229 (NSCLC) tumor microenvironment studies from 309 patients across 19 datasets (32). This analysis
230 revealed a significant correlation between ARG1 and IL6R expression in neutrophils, consistent with
231 the hypothesis that ARG1 expression in neutrophils is driven by IL-6 receptor ligation and signaling
232 (**Figure 5C).**

233 Finally, we cocultured human peripheral blood-derived CD15+CD16+CD66B+CD14- neutrophils
234 (**Supplemental Figure 3G**) with human lung fibroblasts. After 24 hours of coculture, we removed the
235 neutrophils, which are nonadherent cells, and measured collagen expression in the fibroblasts by

236 immunofluorescence. Notably, neutrophil coculture increased fibroblast collagen expression compared
237 to fibroblast monoculture, and this increase could be blocked by IL6-R blockade with tocilizumab
238 (**Figure 5D**). Notably, ARG1 and ornithine levels in the conditioned media were suppressed by
239 tocilizumab (**Figure 5E-F**). Taken together, these analyses support the relevance of fibroblast IL-6-
240 dependent ARG1 expression in the human lung fibrotic niche.
241
242 ***eATP signaling induces fibroblast IL-6.*** To directly test whether the eATP receptor P2rx4 regulates
243 fibroblast IL-6 expression, we considered that myeloid cells including both macrophages and
244 neutrophils can be a source of eATP (33). Thus, we performed scRNAseq of fibroblasts cocultured with
245 macrophages or cultured alone. Interestingly, coculture increased fibroblast expression of IL-6 (**Figure**
246 **6A**), and GO analysis confirmed that the GO pathway "Cellular Response to ATP" was enriched in
247 fibroblasts in coculture compared to monoculture (**Figure 6B**). Importantly, IL-6 was higher in the
248 conditioned media of WT macrophages cocultured with WT versus P2rx4 knockout (KO) fibroblasts
249 (**Figure 6C**). Furthermore, direct treatment of cultured murine lung fibroblasts with ATPγS, a
250 nonhydrolyzable form of ATP, increased IL-6 in the conditioned media of WT but not P2rx4 KO lung
251 fibroblasts, and this effect was blocked by inhibition of p38 Map Kinase, which has been shown to
252 mediate signaling downstream of P2rx4 (34, 35) (**Figure 6D**). To evaluate these results *in vivo*, we
253 tested mice with fibroblast-specific P2rx4 knockout (KO) after bleomycin injury. We found reduced IL-6
254 levels in the bronchoalveolar lavage fluid of KO compared to WT mice (**Figure 6E)**. Furthermore,
255 siRNA KD of P2RX4 in human lung fibroblasts decreased IL-6 expression in response to ATPγS
256 (**Figure 6F)**. We also found that P2rx4 expression increased post-bleomycin injury (**Supplemental**
257 **Figure 3H**), consistent with increased functional effects of this pathway during fibrogenesis. Finally,
258 coculture of human peripheral blood-derived neutrophils with human lung fibroblasts increased IL-6 in
259 the conditioned media compared to fibroblasts or neutrophils alone. This effect could be inhibited by
260 treatment with a small molecule inhibitor of P2rx4 (BAY-1797(36); **Figure 6G**). Taken together, our
261 findings indicate that, in both murine and human systems, eATP-P2rx4 signaling regulates fibroblast IL-

262 6 expression, which in turn induces myeloid Arg1 resulting in ornithine loading of fibroblasts for proline
263 synthesis and pathologic collagen expression.
264
265 **Discussion**
266 For the first time to our knowledge, we demonstrate that Arg1 and its enzymatic product ornithine have
267 a profibrotic effect by driving fibroblast proline synthesis, a key substrate for collagen expression.
268 Imaging studies indicated that ARG1 is expressed more highly in IPF than in healthy human lung
269 explants. Studies using both genetic deletion and chemical inhibition demonstrated the profibrotic effect
270 of Arg1 in murine lung injury and in IPF precision-cut lung slices. Remarkably, we found that the
271 reaction product of Arg1, ornithine, was increased in fibrotic lung tissue from mice and IPF patients.
272 These data build on the recent findings that ornithine was the only amino acid to be elevated in plasma
273 of 100 IPF patients compared to 300 healthy controls (37) and that the expression of ornithine
274 aminotransferase, which converts ornithine to the proline precursor P5C, was correlated with areas of
275 fibrosis in IPF lung (38). Furthermore, we found that ornithine had a profibrotic effect: Ornithine directly
276 increased collagen expression *in vivo* and in cultured murine and human lung fibroblasts. Metabolic
277 labeling studies revealed that ornithine was a substrate for proline synthesis.
278 Our findings also address how this profibrotic amino acid metabolism was initiated via paracrine
279 crosstalk. In both murine and human fibrotic lung and coculture systems, myeloid Arg1 expression was
280 dependent on IL-6 expression in fibroblasts, which in turn was regulated by eATP-P2rx4 signaling. The
281 recent literature has revealed a subset of fibroblasts expressing inflammatory genes in fibrosis,
282 including cytokines (7, 8). A pathologic function of fibroblast-derived cytokine expression is elucidated
283 by our discovery that fibroblast IL-6 is necessary for Arg1 expression in myeloid cells, with the
284 profibrotic consequence of ornithine loading of fibroblasts leading to increased collagen production.
285 The role of type 2 inflammation in fibrosis deserves mention with respect to Arg1. In
286 schistosomiasis-induced fibrosis models, where Arg1 deletion led to an increase in type 2 inflammation
287 and consequently increased fibrosis because of an accumulation of arginine, which supports CD4 T cell
288 proliferation (39). However, in IPF and in murine bleomycin-induced pulmonary fibrosis, type 2

289 inflammation does not appear to be an important driver of fibrosis: Inhibition of type 2 inflammation with
290 dual IL-4 and IL-13 blockade failed to show efficacy in a clinical trial of IPF (40). Furthermore, in the
291 bleomycin-induced sterile injury model that we have used, the onset of type 2 inflammation is later than
292 the period when significant collagen deposition has already occurred and is therefore less relevant to
293 fibrogenesis (41). Therefore, we conclude that type 2 inflammation may be less important in the model.
294 The myeloid cell type expressing Arg1 varied by species. In mice, we found that Arg1 was
295 predominantly expressed in CD11b+CD64+ macrophages and not in canonical Ly6G+ neutrophils.
296 However, there was Arg1 expression in a relatively smaller population of Ly6G+CD64+CD11c+ cells,
297 which may be an intermediate inflammatory myeloid lineage similar to a profile that others have
298 recently described in the setting of murine influenza infection (42). Future studies should more deeply
299 profile these latter cells and ARG1+ cells from IPF, which expressed neutrophil markers, to determine
300 whether they are phenotypically similar. Nonetheless, in both species we confirmed a P2RX4 – IL-6 –
301 ARG1, myeloid-mesenchymal circuit that is functionally important in lung fibrosis. Notably, blood and
302 bronchoalveolar lavage neutrophilia has been associated with fibrosis progression and worse prognosis
303 in IPF (20-23). Our work highlights ARG1 and ornithine metabolism as a neutrophil-dependent pathway
304 that should be developed as a potential therapeutic target for IPF.
305 There are limitations that should be considered when interpreting our results. First, our
306 metabolomic studies indicate conversion of ornithine to proline, a key substrate for collagen synthesis;
307 however, we note that ornithine conversion to polyamines with profibrotic potential remains a further
308 possibility not yet addressed by our results. Second, Arg2 is another arginase that could also contribute
309 to ornithine loading of fibroblasts, and future studies should focus on how both arginases are regulated
310 across the temporal phases of fibrosis. Third, our findings are agnostic with respect to the site of
311 ornithine generation; we detected Arg1 both in both lysates and conditioned media of IL-6-treated
312 macrophages, consistent with the possibility of both intracellular ornithine production and export as well
313 as extracellular production, as per published reports (43, 44). Finally, regarding sources of eATP, we
314 concede that it is likely that multiple sources of eATP exist in the fibrotic niche, such as dying or
315 dysfunctional cells, in addition to myeloid cells themselves. Our results nonetheless reveal that the

316 DAMP signal eATP triggers expression of fibroblast IL-6, which induces profibrotic Arg1 in neighboring
317 myeloid cells.
318 In conclusion, we show the dependence of lung fibrosis on ornithine deriving from myeloid Arg1
319 in mouse models and in functional studies of IPF lung. The importance of understanding the
320 contribution of amino acid metabolism to fibrosis has been recognized in recent years (45), and our
321 findings highlight the role of its immune regulation in the synthesis of pathologic collagen. These
322 studies increase enthusiasm for targeting ARG1 as a therapeutic approach in IPF.
323
324

325 **Methods**

326 ***Sex as a biological variable.*** For preclinical in vivo studies, we used both female and male mice, and
327 experimental groups were balanced with respect to sex. Human lung samples were acquired from both
328 males and females.

329 ***Human lung tissues.*** IPF lung samples were obtained as explants at the time of lung transplantation.
330 Deceased donor-control lungs not known to have lung disease were made available by Donor Network
331 West. Demographic data with respect to ethnicity and race (**Supplemental Table 1**) were derived from
332 the electronic medical record and classified as per NIH notice NOT-OD-15-089.

333 ***Mice.*** Pdgfrb-Cre(46), Lysm-Cre (47), P2rx4 floxed (48), Arg1 floxed (49), Col1a1-EGFP (50), Arg1-
334 RFP-CreERT2 (51), and Arg1-YFP (52) mice were available to the investigative team, and IL-6 KO
335 (53), WT, and R26-LSLS-TdTomato mice were obtained from JAX. Col1a1-GFP mice were obtained
336 from David Brenner (50). All mice were maintained on a C57BL/6 background and were maintained in
337 specific pathogen-free animal barrier facility at the University of California, San Francisco. All
338 experiments were performed on 6-8 weeks old, sex-matched mice.

339 ***Mouse lung injury.*** For lung injury, mice anesthetized with isoflurane were instilled intratracheally with
340 bleomycin (Fresenius, 3U/kg). In the case of Arg1 inhibition, bleomycin-injured mice were treated daily
341 from day 9 to day 15 post-injury with 100 mg/kg CB-1158 (Numidargistat dihydrochloride, HY-101979A,
342 MedChemExpress) dissolved in water, by oral gavage. In the case of ornithine treatment, mice were
343 treated twice daily by gavage with ornithine 2 g/kg dissolved in 100 mL of water.

344 ***Murine macrophage-fibroblast coculture.*** We prepared cocultures of macrophages and fibroblasts
345 that were isolated from the lungs of mice 7 days after bleomycin lung injury. To make single cell
346 suspensions, lungs were harvested from euthanized mice and minced with scissors, and the tissue was
347 resuspended in RPMI with 0.2% Collagenase (10103586001, Roche), 2000 U/ml DNase I
348 (4716728001, Roche), and 0.1 mg/ml Dispase II (4942078001, Sigma). The suspension was incubated
349 for 1 hour at 37°C and then passed through a 70 μm filter (130-110-916, MACS SmartStrainers) to
350 obtain single cells. The cells were washed twice with 1X PBS pH 7.4 (10010023, Gibco). For
351 macrophage isolation, a total of 10^7 cells were resuspended in 80μl PBS buffer supplemented with

352 0.5% BSA (0332, VWR Life Science) and 2mM EDTA (E57040, Research Products International). 20μl
353 CD11b microbeads were used per 10^7 cells. Macrophages were obtained by positive selection by
354 binding to CD11b microbeads and passing through MACS columns (130-049-601, Miltenyi Biotech).
355 Isolated $CD11b^+$ macrophages were cultured in DMEM supplemented with 10% FBS, 1% penicillin-
356 streptomycin (GIBCO), and 20 ng/ml M-CSF (315-02, Peprotech) for 2 days. Primary mouse lung
357 fibroblasts were freshly isolated after magnetic bead-based negative selection of epithelial cells
358 (118204, Biotin anti-mouse CD326 Epcam, Clone: G8.8, BioLegend), endothelial cells (102404, Biotin
359 anti-mouse CD31, clone: 390), immune cells (103104, Biotin anti-mouse CD45, clone: 30-F11,
360 BioLegend), pericytes and smooth muscle cells (134716, Biotin anti-mouse CD146, clone: ME-9F1,
361 BioLegend), and red blood cells (116204, Biotin anti-mouse Ter119, clone: TER-119, BioLegend) with
362 biotinylated antibodies and Dynabeads (MyOne Streptavidin T1, 65601, Thermo Fisher Scientific) as
363 previously described (7). Fibroblasts were cultured for 5 days prior to trypsinization and addition to
364 macrophages for coculture at a 1:1 ratio in DMEM complete media for 5 further days.
365 ***Human lung fibroblast isolation.*** Human lung tissue from deceased donors not used for transplant
366 was resected and minced in Hanks' Balanced Salt Solution (HBSS) buffer supplemented with 0.2%
367 Collagenase (10103586001, Roche), 2000 U/ml DNase I (4716728001, Roche), 0.1 mg/ml Dispase II
368 (4942078001, Sigma), and 1% Penicillin-streptomycin for 1.5 hours at 37°C and 5% CO2. 1X
369 Amphotericin B (15290026, Gibco) was added to the dissociation solution for the last 30 min. Digested
370 lung tissue was lysed further with a MACS tissue dissociator (gentleMACS Dissociator, Miltenyi Biotec)
371 using gentleMACS C tubes (130-093-237, Miltenyi Biotec) at mLUNG-01 setting. The suspension was
372 then passed through a 70 μm filter to obtain single cells. Cells were resuspended in PBS with 0.5%
373 BSA and 2mM EDTA. For the negative selection of human fibroblasts, the following antibodies were
374 used at a 1:200 ratio: epithelial cells (324216, Biotin anti-human Epcam, clone:9C4, BioLegend),
375 endothelial cells (13-0319-82, Biotin anti-human CD31, clone: WM-59, Invitrogen), immune cells
376 (368534, Biotin anti-human CD45, clone: 2D1, BioLegend), and pericytes and smooth muscle cells
377 (361036, Biotin anti-human CD146, clone: P1H12, BioLegend). Fibroblasts were cultured in DMEM
378 supplemented with 10% serum, 1% penicillin-streptomycin, and 1% amphotericin B for a total of 5 days.

379 ***Human neutrophil isolation and coculture with fibroblasts.*** Whole blood (10ml) from heathy donors
380 was collected in BD Vacutainer® k-EDTA Tubes (Vitalant, San Francisco, CA) and used for primary
381 neutrophil isolation as previously described (54). Briefly, 7ml blood was layered on top of 7ml of
382 PolymorphPrep (Cosmo Bio Usa Inc, AXS-1114683) and centrifuged at 500 x *g* for 35 min at room
383 temperature without braking. The peripheral blood mononuclear cells and plasma layers were aspirated
384 and the neutrophil layer was collected. The cells were washed with PBS and centrifuged at 400g for 5
385 minutes. The cell pellet was resuspended in 3ml ACK lysis buffer (Thermo Fisher, A1049201) and
386 centrifuged at 400g for 5 minutes. Neutrophil purity was 95%, confirmed by flow cytometry
387 (**Supplemental Figure 3F;** Antibodies: CD15 clone W6D3, Biolegend cat# 323039; CD66B clone
388 G10F5, Biolegend cat# B221034; CD16 clone 3G8, BD Biosciences cat# 560474; CD14 Clone 63D3,
389 Biolegend cat# 367118). The cells were finally resuspended in RPMI supplemented with 10% FBS and
390 counted. Neutrophils were then added to human lung fibroblasts for 24 hours of coculture in RPMI with
391 10% FBS, with or without P2RX4 inhibitor BAY-1797 (1 μm, 7573, Tocris) or IL6-R blocking antibody
392 tocilizumab (100 ng/mL, HY-P9917, MedChemExpress). The conditioned media were retained for
393 analysis after separation of the cellular fraction by centrifugation, and fibroblasts were fixed and
394 permeabilized for immunofluorescence analysis.
395 ***Flow cytometry and sorting.*** *Cocultured cells:* Cocultures were trypsinized with 0.25% trypsin and
396 resuspended in 1X PBS with 0.5% BSA and 2mM EDTA. Single-cell suspensions were pre-stained with
397 Fc blocker for 10 min in ice followed by staining at 1:300 with anti-CD64 (139304, PE anti-mouse
398 CD64, clone:X54-5/7.1, BioLegend) and anti-Pdgfra (25-1401-82, PE-Cy7, anti-mouse CD140a, clone:
399 APA5, Invitrogen) antibodies for 40 min. DAPI was used to distinguish dead cells. *Mouse lung cell*
400 *suspensions:* Whole lung single cell suspensions were prepared by harvesting lung lobes into 5 ml
401 HBSS with 40μl Liberase Tm (0.1 U/ml, 5401127001, Roche) and 20μl DNAse 1 (10mg/ml, Roche,
402 Cat# 10104159001), followed by automated tissue dissociation (GentleMacs; Miltenyi Biotec) and
403 tissue digestion for 30 min at 37°C on a shaker. Digested samples were processed on the GentleMacs
404 using the “lung2” program, passed through 70μm filters, and washed, followed by red blood cell lysis
405 and final suspension in FACS buffer. Cells were counted using a NucleoCounter (Chemometic). All

406 samples were stained in 96-well V-bottom plates. Single cell samples were first incubated with
407 antibodies to surface antigens for 30 min at 4°C in 50µl staining volume. Flow cytometry was performed
408 on BD LSRFortessa X-20. Fluorochrome compensation was performed with single-stained UltraComp
409 eBeads (Invitrogen, Cat# 01-2222-42). Samples were FSC-A/SSC-A gated to exclude debris, followed
410 by FSC-H/FSC-A gating to select single cells and Draq7 viability dye (Biolegend) to exclude dead cells.
411 Monocyte-derived macrophages (moMacs) were identified as $CD19^-$, $Ly6G^-$, $NK1.1^-$, $Siglec\text{-}F^-$, $CD11b^+$,
412 and $CD64^+$. Arginase1-positive cells were identified by the presence of eYFP. Data were analyzed
413 using FlowJo software (TreeStar, USA) and compiled using Prism (GraphPad Software). Monoclonal
414 antibodies used were: anti-CD45 (30-F11, Biolegend), anti-CD11b (M1/70, Biolegend), anti-CD11c
415 (N418, Biolegend), anti-NK1.1 (PK136, Biolegend), anti-CD19 (6D5, Biolegend), anti-CD64 (X54-5/7,
416 eBiosciences), anti-Ly6G (1A8, Biolegend), anti-SiglecF (E50-2440), anti-I-A/I-E (MHCII) (M5/114.15.2,
417 Biolegend), and anti-CCR2 (475301, BD BioSciences). In the case of quantifying and sorting
418 CD45+CD11b+CD64+ monocyte-derived macrophages in bleomycin-injured WT and IL-6 KO mouse
419 lung cell suspensions, 50,000 microbeads (Invitrogen) were added to each sample for quantification of
420 absolute live CD45+CD11b+CD64+ cells. Lavage cell pellets were added to the suspensions prior to
421 sorting. Cells were sorted on a FACS Aria2.
422 ***Quantitative Real-Time PCR analysis.*** Human lung fibroblasts were lysed in 300µl TRIzol reagent
423 (10296010, Ambion life technologies) to obtained RNA. 600 ng of RNA per sample was used to prepare
424 cDNA using iScript reverse transcriptase supermix (Bio-Rad, 1708841). qPCR was performed for the
425 target genes using SYBR Green super mix (Applied Biosystems, 4309155). Gene expression was
426 normalized to 18S rRNA. The following primers were used:
427 P2RX4 Forward: GAGATTCCAGATGCGACCACT
428 P2RX4 Reverse: ACCCGTTGAAAGCTACGCAC
429 18S rRNA Forward: GTAACCCGTTGAACCCCATT
430 18S rRNA Reverse: CCATCCAATCGGTAGTAGCG

431 In the case of sorted CD45+CD11b+CD64+ murine lung monocyte-derived macrophages, mRNA was
432 isolated form pelleted cells as above, and qPCR was performed. Gene expression was normalized to
433 Gapdh. The following primers were used:
434 Arg1 Forward: CTCCAAGCCAAAGTCCTTAGAG
435 Arg1 Reverse : AGGAGCTGTCATTAGGGACATC
436 Gapdh Forward: AGTATGACTCCACTCACGGCAA
437 Gapdh Reverse: TCTCGCTCCTGGAAGATGGT
438 ***siRNA Knockdown.*** Healthy human fibroblasts were treated with 5μM siRNA (Dharmacon, D-001810-
439 01-05 ON-TARGET plus No-targeting siRNA) control or (Dharmacon, L-006285-00-0010 ON-TARGET
440 plus Human P2RX4 SMARTpool) using DharmaFECT in serum-free media for 12 hours, followed by
441 supplementing with DMEM with 10% serum. Cells were incubated for an additional 48 hours. Treated
442 cells were harvested for either RNA isolated or stimulated with 100μM ATPγS for 12 hours and culture
443 supernatant was collected for Human IL6 ELISA assay.
444 ***IL-6 ELISA.*** Bronchoalveolar lavage fluid from mice or conditioned media from cultured murine cells
445 were collected for measurement of IL-6 with a Duoset ELISA kit (R&D Systems, DY406-05).
446 Conditioned media from cultured human cells were collected and IL-6 was measured using Duoset
447 ELISA kit (R&D Systems, DT206-05). In both cases, the capture antibody was coated overnight in a 96-
448 well plate at room temperature. Wells were aspirated and washed in ELISA wash buffer and blocked by
449 adding reagent diluent consisting of 1% BSA in PBS. After 1 hour of room temperature incubation, wells
450 were again washed with wash buffer and samples or standards were added and incubated for 2 hours
451 at room temperature. Detection antibody was used along with streptavidin-HRP and substrate solution.
452 The reaction was stopped with stop solution, and optical density was measured using a microplate
453 reader at 450 nm.
454 ***Arginase 1 ELISA.*** *Mouse:* Arginase 1 levels were measured from conditioned media or from
455 bronchoalveolar lavage, using Mouse Arginase 1 ELISA Kit (ab269541, Abcam) based on the
456 manufacturer's protocol. Briefly, CD11b+ mouse lung cells were seeded in 12-well dishes for 2 days in
457 DMEM supplemented with M-Csf (315-02, Peprotech). Cells were exposed to murine IL-6 for 72 hours,

458 and culture supernatant and cell lysate were then collected. For *in vivo* experiments, bleomycin-injured
459 mice received bronchoalveolar lavage with 1 mL of PBS on day 14 after injury, and the noncellular
460 fraction was retained for analysis. For the ELISA, subsequently, 50 µl of undiluted samples were added
461 to each well, along with a 50 µl antibody cocktail comprising capture antibody and detection antibody
462 dissolved in antibody diluent. Plates were incubated for 1 hour at room temperature. Wells were
463 washed thrice with wash buffer and incubated with 100 µl Tetramethylbenzidine (TMB) substrate for 15
464 min. The reaction was stopped using 100µl stop solution, and OD was measured at 450nm. *For*
465 *Human:* Arginase 1 levels were measured from IPF precision-cut lung slice (PCLS) using the Human
466 Arginase 1 ELISA Kit (BMS2216, ThermoFisher), following the manufacturer's instructions. Briefly,
467 following 24 hours of culture with or without tocilizumab (100 ng/mL, HY-P9917, MedChemExpress),
468 PCLS were lysed in RIPA buffer with protease inhibitor, and 100 µl of standards or undiluted sample
469 was added to each well of a pre-coated 96-well plate and incubated for 2 hours at room temperature.
470 Wells were then washed four times with provided wash buffer before the addition of 100 µl of biotin-
471 conjugated anti-arginase 1 antibody to each well, followed by a 1-hour incubation. After another wash
472 step, 100 µl of streptavidin-horseradish peroxidase (HRP) was added and incubated for 30 minutes.
473 Wells were washed again and incubated with 100 µl of TMB substrate solution for 15 minutes. The
474 enzymatic reaction was stopped by adding 100 µl of stop solution, and optical density (OD) was
475 measured at 450 nm using a microplate reader.
476 ***Histology and Immunofluorescence imaging.*** *Mouse lung:* Arg1-RFP-creERT2 /Rosa26-LSL-
477 TdTomato/Col1a1-EGFP mice were injured for 14 days. Lungs from uninjured or injured mice were
478 inflated with a solution consisting of 30% sucrose solution mixed 1:1 with OCT (4585, OCT) and fixed in
479 4% formaldehyde at 4°C for 4 hours. Lungs were then washed and submerged in 30% sucrose solution
480 overnight at 4°C. Next, the tissue was incubated in the 1:1 solution of 30% sucrose and OCT overnight
481 followed by changing to OCT for 2 hours, and then a tissue block was frozen after embedding in OCT.
482 5 µm sections were cut from OCT-embedded tissue. For immunofluorescence imaging, frozen sections
483 were incubated with Mertk antibody (AF591, R&D Systems) or S100A8 antibody (AF3059, R&D
484 Systems) in staining buffer (1% BSA, 0.5% Triton x-100 in PBS), washed, and then incubated with

485 anti-rabbit secondary antibody (Invitrogen). Slides were washed with PBS and mounted on antifade
486 DAPI mounting media. *Human lung:* 5 μm thick sections from patient FFPE blocks were collected for
487 IHC staining. Slides were stained using Opal Manual IHC kit (PerkinElmer). After deparaffinization,
488 antigen retrieval was performed in AR buffer for 45 sec at 100% power followed by 15 min at 20%
489 power. After blocking slides were incubated with primary antibodies ARG1 (Cat# 93668, Cell Signaling
490 Technology) overnight at 4C. Polymer HRP was introduced to slides for 10 min, followed by signal
491 amplification using Opal570 (NEL810001KT,Akoya Biosciences) for 10 min at room temperature. The
492 slides were then counterstained with DAPI mounting media and scanned using with a 10x and 40x
493 objective of Leica inverted widefield microscope. *Cultured Cells:* Macrophages and fibroblasts or
494 fibroblasts alone, isolated from mouse lung as detailed above, were cultured on glass coverslips and in
495 some cases treated with CB-1158 (1 μM), ornithine (1 mM), or 1 μM OAT inhibitor 5-FMOrn
496 dihydrochloride (HY154021A, MedChemExpress). Cells were fixed with 4% PFA, permeabilized with
497 1% BSA, 0.5 % triton x-100 in PBS, and incubated with primary antibodies (Col1a1, #720265, Cell
498 Signaling Technology; α-SMA, A5228, Sigma) followed wash, secondary antibodies, further wash, and
499 mounting. Imaging was performed on a Leica SP8 laser scanning confocal microscope. Fluorescence
500 signal was quantified with Imaris software for cellular areas.
501 ***Western blot.*** Precision cut lung slices were obtained from human IPF tissue sections. Briefly, IPF
502 tissue was injected with 2% low melting agarose (50111, Lonza) and then submerged in ice-cold PBS
503 to allow solidification of agarose. 400 µm lung slices was generated using a Compresstome device (VF-
504 310-OZ, Precisionary Instruments). Slices were kept in complete DMEM media for 2 hours to allow the
505 release of agarose followed by changing to fresh complete DMEM with 10% FBS and 1% penicillin-
506 streptomycin. Lung slices were treated with 50 μM CB-1158 for 24 hours. After incubation slices were
507 minced using a tissue homogenizer. Cells were lysed in Pierce RIPA buffer (Thermo Fisher Scientific,
508 89901) with protease inhibitor cocktail (Thermo Fisher Scientific, 1861278). 10 µg of protein was run on
509 10% sodium dodecyl sulfate-polyacrylamide gel electrophoresis (Bio-rad, 4561034) and transferred to a
510 PVDF membrane (Thermo Fisher Scientific, 88520). The membrane was incubated with 1:1000 Col1a1
511 antibody (#720265, Cell Signaling Technology) overnight at 4°C. Blots were washed in 1X TBST and

512 incubated with peroxidase-conjugated goat anti-rabbit (1:20,000, Anaspec, AS28177) for 4 hr at 4°C.
513 These blots were developed using SuperSignal West Pico Chemiluminescent substrate (Thermo Fisher
514 Scientific, 34080) in ChemiDoc XRS+ gel imaging system (Bio-rad). Quantification of bands was done
515 using ImageJ.
516 ***Hydroxyproline assay.*** Mice were euthanized and lungs were excised and snap-frozen. Isolated lung
517 samples were homogenized and incubated with 50% trichloroacetic acid (T6399, Sigma) on ice for 20
518 min. Samples were then incubated in 12N HCL (A144, Fisher) overnight at 110°C. Dried pellets were
519 reconstituted in distilled water with constant shaking for 2 hours at room temperature. Samples were
520 then mixed with 1.4% Chloramine T (Sigma, 85739) and 0.5 M sodium acetate (Sigma, 241245) in 10%
521 2-propanol (Fisher, A416) and incubated with Ehrlich's solution (Sigma, 03891) for 15 min at 65°C.
522 Absorbance was quantified at 550 nm, and concentration was calculated using a standard curve of
523 commercial hydroxyproline (Sigma, H5534).
524 ***scRNAseq library preparation and sequencing.*** PIPseq T2 3' Single Cell RNA Kit (v3.0 – cultured
525 cells, v4.0 – directly sequenced cells) was used for pre-templated instant partitioning (PIP) to capture
526 single-cell mRNA transcripts with PIP beads according to manufacturer's protocol (Fluent Biosciences,
527 FB0001026). After 5 days of coculture, single cell suspension of cells was obtained by trypsinization
528 followed by washing in 1X PBS. Cells were washed in ice-cold PIPseq Cell Suspension Buffer (Fluent
529 Biosciences, FB0002440). Cells were counted and stained with Trypan blue to confirm >90% viability.
530 Single-cell library preparation was performed using the manufacturer-recommended default protocol
531 and settings. The sequencing libraries were submitted to UCSF Center for Advanced Technology
532 (Novaseq X) or Novogene (Novaseq 6000) for sequencing. The demultiplexed FASTQ files were
533 aligned to mouse genome (mm10) using PIPseeker 1.0.0 (Fluent Biosciences). After sequence
534 alignment, we observed around 50% of input cells being called when PIPseeker sensitivity level was
535 set to 3, which was near the inflection point of the barcode rank plot. The original FASTQ files, the
536 quality reports, and the expression matrix outputs of PIPseeker have been deposited in Gene
537 Expression Omnibus (GEO).

538 ***scRNAseq Data Analysis.*** The Seurat – Guided Clustering Tutorial (March 27, 2023) was followed to
539 convert our expression matrixes into Seurat objects (Seurat version 4.3.0) (55). For quality control, we
540 removed the cells with less than 200 genes or more than 10,000 genes and larger than 5%
541 mitochondrial content. Seurat objects were integrated following Seurat's Introduction to scRNAseq
542 Integration (March 27, 2023), selecting the top 2,000 variable features as integration anchors. Cell
543 doublets were removed with the package DoubletFinder (2.0.3) (56). Following Seurat – Guided
544 Clustering Tutorial (March 27, 2023), we selected the top 2000 highly variable genes to obtain the cell
545 UMAP coordinates and group the cells into clusters with a sensitivity of 0.5(55). Cell types were
546 annotated using the SingleR package 1.10.04(2) using the ImmGen database (57) as reference. The
547 Gene Set Enrichment Analysis (GSEA) was performed using the package enrichR 3.1(58) (FDR<0.05),
548 with gene ontology data taken from the database "GO_Biological_Process_2021"(59). Cell
549 communication pathways analysis was performed using the package CellChat (1.6.1) (27). Upstream
550 regulator prediction was done using the Ingenuity Pathway Analysis software (Qiagen) (60).
551 Differentially expressed genes for macrophages with $p < 0.05$ and average log2 fold change > 0.75
552 were used for analysis. Analysis results with $p < 0.05$ were considered significant.
553 ***Multiplexed Ion Beam Imaging and Analysis (MIBI).*** *Slide Preparation:* Serial 5 um FFPE sections
554 were cut onto one glass and one gold slide. Both slides were baked at 70* Celsius overnight and
555 deparaffinized in three washes of fresh Xylene and rehydrated in EtOH (2X 100% EtOH, 2X 90% EtOH,
556 1X 80% EtOH, 1X 70% EtOH) and distilled water (2X) washes. Washes were performed in (include
557 wash machine specs). An antigen retrieval slide chamber was prepared by diluting 10X Tris with EDTA
558 antigen retrieval buffer 1:10 in diH2O. The prepared slide chamber was added to a PT Module (add
559 specs) filled with PBS and preheated to 75ºC. The rehydrated slides were run in the preheated PT
560 module at 97ºC for 40 minutes, then cooled to 65ºC in the PT module. The prepared slide chamber was
561 then removed from the PT module and cooled at RT for 30 minutes. Slides were washed 2X in 1X TBS-
562 Tween. *Glass Slide IHC:* Tissues were encircled by PAP pen boarders and blocked with 5% donkey
563 serum diluted in TBS IHC wash buffer for 1 hour at RT in a moisture chamber. Wash buffer was
564 aspirated from the slide, and Arginase-1 primary antibody (Ionpath Cat#: 715001) was stained

565 overnight at 4ºC overnight in the moisture chamber. The following day, primary antibody was aspirated,
566 and slides were washed twice with 1X TBS-T for 5 minutes, blocked with 3% peroxide buffer for 15
567 minutes at RT, and washed again twice with 1X TBS-T for 5 minutes each wash before incubation with
568 anti-rabbit secondary antibody for 1 hour at RT. Slides were washed twice with 1X TBS-T for 5 minutes
569 before visualization with 100uL DAB for 5 minutes at RT. DAB reaction was stopped by tapping waste
570 into contained waste bin, and then washing the slide into a slide chamber filled with diH2O 3X for 30
571 seconds each wash. The slide was then stained with Hematoxylin for 1 minute at RT and washed with
572 tap water 2X for 30 seconds. The slide was then dehydrated by washing in EtOH (1X 70% EtOH, 1X
573 80% EtOH, 2X 95% EtOH, 2X 100% EtOH), and Xylene (2X) before cover slipping. *Gold Slide Staining:*
574 Gold slides were transferred the Sequenza Immunostaining Center Staining System (Electron
575 Microscopy Sciences, Hatfield, PA). Endogenous biotin-binding proteins with blocked with
576 (Avidin/biotin-blocking reagents) for 30 minutes at room temperature. 5% donkey serum was added to
577 the top of the chamber to wash out the avidin blocking reagents and block additional non-specific
578 antibody binding sites for 1 hour at RT. Primary and Secondary antibodies panels were assembled with
579 appropriate volumes of each titrated antibody and a final concentration of 0.05M EDTA. The complete
580 cocktails were filtered through a pre-wet 0.1 um Ultragree MC Spin Filter, and then the Primary
581 Antibody cocktail (**Supplemental Table 2**) was added to the Sequenza top chamber and incubated
582 overnight at 4ºC. The Secondary antibody cocktail was stored at 4ºC. The following day, the slides
583 were washed by adding 1X TBS-T to the Sequenza chamber 2X before adding the Secondary Antibody
584 cocktail to the Sequenza chamber for 1 hour at RT. Gold slides were removed from the Sequenza
585 chamber and washed 3X with 1X TBS-T for 5 minutes each wash, 1X with filtered 2% Glutaraldehyde
586 for 5 minutes, 3X with filtered 1X Tris pH 8.5, 2X with filtered diH2O, 1X with 70% EtOH, 1X with 80%
587 EtOH, 2X with 90% EtOH, and 2X with 100% EtOH. Slides were allowed to dry at RT for 10 minutes
588 before being stored in a vacuum chamber (Cat#) before MIBIscope analysis. *Image Acquisition and*
589 *Processing:* Gold slides were loaded into the MIBIscope (Ionpath, Menlo Park, CA) and FOVs were
590 selected by matching tissue topography to ROIs with Arginase-1+ Staining from the serial IHC glass
591 slide. FOVs were acquired at Fine resolution, with a dwell time of 1 second at a resolution of 0.39 um

592 per pixel. Image QC was performed by following the Angelo Lab toffy pipeline
593 (https://github.com/angelolab/toffy). Analysis was performed by following the Angelo Lab ark pipeline
594 (https://github.com/angelolab/ark-analysis).
595 ***Spatial Transcriptomics (10x Xenium).*** FFPE preserved sections of lung tissue were prepared for
596 spatial transcriptomics imaging on the Xenium platform by following 10x Genomics protocols
597 CG000582 Rev E and CG000584 Rev A. Briefly, protocol CG000582 prepares the slides for the
598 imaging run by first hybridizing the probe panel of choice. Here, the standard human lung panel
599 available from 10x Genomics (Cat #1000601) was supplemented with a custom panel specific for lung
600 disease states, including pulmonary fibrosis (**Supplemental Table 3**). Following probe hybridization,
601 annealed probes are ligated together to create circular fragments, then circularized probes are
602 amplified with a rolling circle PCR. After rolling circle amplification, slides are DAPI stained for nuclei
603 then placed in the Xenium Analyzer with run reagents following CG000584. The gene panel is
604 uploaded to the Xenium Analyzer and a primary image is take of the slides. All areas with visible tissue
605 are selected for imaging and the imaging run is started. The Xenium processes imaging data during the
606 run, identified cell boundaries and outputting image files along with cell by transcript by location
607 matrices for further downstream analysis by Seurat 10x Xenium protocol. *Proximity Analysis of ARG1+*
608 *cells and IL6+ fibroblasts:* The output files of Xenium Analyzer were converted to an AnnData object
609 that contained the cell centroid coordinates and raw transcript counts. A filter of 10 counts per cell and
610 5 cells per gene was applied to filter out low-quality cells and sparsely detected genes. Counts were
611 normalized to 1e4 and log-transformed. Cells were then grouped into one of the following three
612 categories: (1) ARG1+; (2) IL6+ARG1- and either CTHRC1 or COL1A1; and (3) IL6+ARG1- and
613 CTHRC1 or COL1A1 , with positive expression of a marker defined as having non-zero counts. *Co-*
614 *occurrence probability ratio:* The 'Analyze Xenium data' tutorial in Squidpy (version 1.5.0) (61) was
615 followed to compute the co-occurrence probability ratio of ARG1+ and fibroblasts as defined above. We
616 performed 50% random subsampling of the data 5 times to compute the statistic and generate
617 confidence intervals bounded by the minimum and maximum probability ratio generated by the
618 subsamples. The co-occurrence probability ratio was computed at 25 μm between cells. Using the

619 implementation in the 1.5.0 release of Squidpy, for each radial distance, the ratio of cells belonging to
620 category exp (exp being any of the three categories of cell defined above) out of all cells within the
621 given distance of an ARG1+ cell was averaged across all ARG1+ cells to compute the conditional
622 probability in the numerator P(exp | ARG1+), while the denominator P(exp) was computed similarly but
623 averaging probabilities that were computed by centering around every cell in the sample. Previous
624 releases of Squidpy implemented a version of this test in the function gr.co_occurrence that used
625 discrete interval bins (only including cells within two consecutive choices of radial distances). We chose
626 to use inclusive intervals (including all cells within a given radial distance) for a more robust calculation
627 of the co-occurrence probability ratio. We implemented our method into the codebase of Squidpy, with
628 the help of Squidpy's authors, and it is now the default implementation of the function
629 gr.co_occurrence, starting in release 1.5.0.
630 ***Analysis of published datasets.*** *Bleomycin time course:* Time series of single-cell data after
631 bleomycin lung injury were obtained from Tsukui et al (8) and Strunz et al (9). These samples were
632 processed and merged with Seurat (4.3.0) using the function SCTransform to correct for batch effects
633 and annotated with SingleR 1.10.044 using the ImmGen database as reference to identify cell types.
634 *Macrophage Annotation in vivo:* We annotated macrophages from Strunz et al. (9) according to the
635 macrophage subtypes (C1, C2, C3) defined by Aran et al (2). and by Li et al (11) using SingleR(2). *BAL*
636 *Microarray:* Microarray RNA data from bronchoalveolar cells of healthy individuals and IPF patients was
637 extracted from the GPL14550 dataset within the GSE70867(12) repository. The differentially expressed
638 genes between IPF and healthy samples were obtained by following the R workflow provided by the
639 NCBI GEO2R platform using GEOquery (2.66.0) and limma (3.54.2) packages. *Gene expression of*
640 *cultured mouse lung-derived macrophages:* The top markers of macrophage subtypes as defined by Li
641 et al. (11) and Aran et al.(2) were quantified in our CD11b+, CSF1-treated macrophages (from the WT-
642 WT coculture condition). *Analysis of lung tumor neutrophils:* A high-resolution single-cell atlas of tumor-
643 associated neutrophils in non-small cell lung cancer was obtained from (32). The scANVI algorithm-
644 based integrated NSCLC transcriptome atlas provided more than 1.2M cells from 19 studies and 309
645 patients. The metadata embedded with Leiden-clustering and cell-type annotations were utilized to

646 identify and subset neutrophils. The subset data was log transformed and scaled, followed by filtering
647 for cells expressing both ARG1 and IL6R. Pearson correlation coefficient, p-value and R-squared
648 values were calculated for the correlation between ARG1 and IL6R.
649 ***Ornithine Measurement.*** Cultured PCLS from IPF explanted lungs lysed in water, IPF lung samples
650 lysed in RIPA buffer, or mouse lung homogenized and lysed in RIPA buffer were used to measure
651 ornithine following manufacturer's protocol (IS I-1000R, Immusmol). Briefly, each sample was
652 precipitated with 50 µL precipitating reagents (provided by manufacturer) followed by extraction using
653 D-reagent (a derivatizing agent provided by manufacturer) for 2h at room temperature. 10 µL of the
654 prepared standards, controls and samples were incubated with 90 µL of antiserum overnight at 4□C.
655 Subsequently, plates were washed and briefly incubated with enzyme conjugate for 30min followed by
656 addition of substate. Absorbance was measured using microplate reader at 450nm.
657 ***LC-MS metabolomics.*** Primary murine lung macrophages and fibroblasts were cocultured with or
658 without 1 µM CB-1158. Fibroblasts were isolated by antibody-coated bead-based negative selection of
659 macrophages. Fibroblast extracts were used to calculate protein equivalents by resuspension in 0.2 M
660 NaOH, heated to 95 °C for 25 min, and determined via BCA (Pierce, 23225). Dried metabolites were
661 resuspended in 50% ACN:water and 1/10th of the volume was loaded onto a Luna 3 um NH2 100A
662 (150 × 2.0 mm) column (Phenomenex). The chromatographic separation was performed on a Vanquish
663 Flex (Thermo Scientific) with mobile phases A (5 mM NH_4AcO pH 9.9) and B (ACN) and a flow rate of
664 200 µL/min. A linear gradient from 15% A to 95% A over 18 min was followed by 9 min isocratic flow at
665 95% A and re-equilibration to 15% A. Metabolites were detected with a Thermo Scientific Q Exactive
666 mass spectrometer run with polarity switching (+3.5 kV / -3.5 kV) in full scan mode with an m/z range of
667 65-975. TraceFinder 4.1 (Thermo Scientific) was used to quantify the targeted metabolites by area
668 under the curve using expected retention time and accurate mass measurements (< 5 ppm). Values
669 were normalized to cell number and sample protein concentration. Relative amounts of metabolites
670 were calculated by summing up the values for all isotopologues of a given metabolite.
671 ***Study Approval.*** Experiments in mice were performed in accordance with approved protocols by the
672 University of California, San Francisco Institutional Animal Care and Use Committee. The studies with

673 human tissues described in this paper were conducted according to the principles of the Declaration of
674 Helsinki. Written, informed consent was obtained from all subjects, and the study was approved by the
675 University of San Francisco, California and Vitalant institutional review board. With respect to deceased
676 donor control explanted lungs, because samples were acquired from deceased individuals the study is
677 not considered human subjects research as per UCSF and NIH policy.
678 ***Statistics.*** One-way ANOVA followed by post hoc Sidak's multiple comparisons tests was used for
679 comparisons among more than two groups, and Student's t-test was used for comparison between two
680 groups. A p value less than 0.05 was considered significant. Analysis appropriately corrects for multiple
681 comparisons and repeated measures.
682 ***Data availability.*** Newly generated single-cell sequencing data will be made public on acceptance for
683 publication at GSE242510.
684
685

686 **References**

687 1. Wolters PJ, Blackwell TS, Eickelberg O, Loyd JE, Kaminski N, Jenkins G, et al. Time for a
688 change: is idiopathic pulmonary fibrosis still idiopathic and only fibrotic? *Lancet Respir Med.*
689 2018;6(2):154-60.
690 2. Aran D, Looney AP, Liu L, Wu E, Fong V, Hsu A, et al. Reference-based analysis of lung single-
691 cell sequencing reveals a transitional profibrotic macrophage. *Nat Immunol.* 2019;20(2):163-72.
692 3. Joshi N, Watanabe S, Verma R, Jablonski RP, Chen CI, Cheresh P, et al. A spatially restricted
693 fibrotic niche in pulmonary fibrosis is sustained by M-CSF/M-CSFR signalling in monocyte-
694 derived alveolar macrophages. *Eur Respir J.* 2020;55(1).
695 4. Riteau N, Gasse P, Fauconnier L, Gombault A, Couegnat M, Fick L, et al. Extracellular ATP is a
696 danger signal activating P2X7 receptor in lung inflammation and fibrosis. *Am J Respir Crit Care*
697 *Med.* 2010;182(6):774-83.
698 5. Bhattacharyya A, Torre P, Yadav P, Boostanpour K, Chen TY, Tsukui T, et al. Macrophage
699 Cx43 Is Necessary for Fibroblast Cytosolic Calcium and Lung Fibrosis After Injury. *Front*
700 *Immunol.* 2022;13:880887.
701 6. Buechler MB, Pradhan RN, Krishnamurty AT, Cox C, Calviello AK, Wang AW, et al. Cross-
702 tissue organization of the fibroblast lineage. *Nature.* 2021;593(7860):575-9.
703 7. Tsukui T, Sun KH, Wetter JB, Wilson-Kanamori JR, Hazelwood LA, Henderson NC, et al.
704 Collagen-producing lung cell atlas identifies multiple subsets with distinct localization and
705 relevance to fibrosis. *Nat Commun.* 2020;11(1):1920.
706 8. Tsukui T, Wolters PJ, and Sheppard D. Alveolar fibroblast lineage orchestrates lung
707 inflammation and fibrosis. *Nature.* 2024;631(8021):627-34.
708 9. Strunz M, Simon LM, Ansari M, Kathiriya JJ, Angelidis I, Mayr CH, et al. Alveolar regeneration
709 through a Krt8+ transitional stem cell state that persists in human lung fibrosis. *Nat Commun.*
710 2020;11(1):3559.

711 10. Fabre T, Barron AMS, Christensen SM, Asano S, Bound K, Lech MP, et al. Identification of a
712 broadly fibrogenic macrophage subset induced by type 3 inflammation. *Sci Immunol.*
713 2023;8(82):eadd8945.
714 11. Li X, Mara AB, Musial SC, Kolling FW, Gibbings SL, Gerebtsov N, et al. Coordinated chemokine
715 expression defines macrophage subsets across tissues. *Nat Immunol.* 2024;25(6):1110-22.
716 12. Prasse A, Binder H, Schupp JC, Kayser G, Bargagli E, Jaeger B, et al. BAL Cell Gene
717 Expression Is Indicative of Outcome and Airway Basal Cell Involvement in Idiopathic Pulmonary
718 Fibrosis. *Am J Respir Crit Care Med.* 2019;199(5):622-30.
719 13. Zhang H, Zhu X, Friesen TJ, Kwak JW, Pisarenko T, Mekvanich S, et al. Annexin
720 A2/TLR2/MYD88 pathway induces arginase 1 expression in tumor-associated neutrophils. *J*
721 *Clin Invest.* 2022;132(22).
722 14. Rotondo R, Barisione G, Mastracci L, Grossi F, Orengo AM, Costa R, et al. IL-8 induces
723 exocytosis of arginase 1 by neutrophil polymorphonuclears in nonsmall cell lung cancer. *Int J*
724 *Cancer.* 2009;125(4):887-93.
725 15. Cane S, Barouni RM, Fabbi M, Cuozzo J, Fracasso G, Adamo A, et al. Neutralization of NET-
726 associated human ARG1 enhances cancer immunotherapy. *Sci Transl Med.*
727 2023;15(687):eabq6221.
728 16. Angelo M, Bendall SC, Finck R, Hale MB, Hitzman C, Borowsky AD, et al. Multiplexed ion beam
729 imaging of human breast tumors. *Nat Med.* 2014;20(4):436-42.
730 17. Keren L, Bosse M, Marquez D, Angoshtari R, Jain S, Varma S, et al. A Structured Tumor-
731 Immune Microenvironment in Triple Negative Breast Cancer Revealed by Multiplexed Ion Beam
732 Imaging. *Cell.* 2018;174(6):1373-87 e19.
733 18. Keren L, Bosse M, Thompson S, Risom T, Vijayaragavan K, McCaffrey E, et al. MIBI-TOF: A
734 multiplexed imaging platform relates cellular phenotypes and tissue structure. *Sci Adv.*
735 2019;5(10):eaax5851.

736 19. Rahim MK, Okholm TLH, Jones KB, McCarthy EE, Liu CC, Yee JL, et al. Dynamic CD8(+) T cell
737 responses to cancer immunotherapy in human regional lymph nodes are disrupted in metastatic
738 lymph nodes. *Cell.* 2023;186(6):1127-43 e18.
739 20. Achaiah A, Fraser E, Saunders P, Hoyles RK, Benamore R, and Ho LP. Neutrophil levels
740 correlate with quantitative extent and progression of fibrosis in IPF: results of a single-centre
741 cohort study. *BMJ Open Respir Res.* 2023;10(1).
742 21. Pitre T, Lupas D, Ebeido I, Colak A, Modi M, Kachkovski GV, et al. Prognostic factors
743 associated with mortality in acute exacerbations of idiopathic pulmonary fibrosis: A systematic
744 review and meta-analysis. *Respir Med.* 2024;222:107515.
745 22. Kono M, Miyashita K, Hirama R, Oshima Y, Takeda K, Mochizuka Y, et al. Prognostic
746 significance of bronchoalveolar lavage cellular analysis in patients with acute exacerbation of
747 interstitial lung disease. *Respir Med.* 2021;186:106534.
748 23. Kinder BW, Brown KK, Schwarz MI, Ix JH, Kervitsky A, and King TE, Jr. Baseline BAL
749 neutrophilia predicts early mortality in idiopathic pulmonary fibrosis. *Chest.* 2008;133(1):226-32.
750 24. Tran DH, Kesavan R, Rion H, Soflaee MH, Solmonson A, Bezwada D, et al. Mitochondrial
751 NADP(+) is essential for proline biosynthesis during cell growth. *Nat Metab.* 2021;3(4):571-85.
752 25. Steggerda SM, Bennett MK, Chen J, Emberley E, Huang T, Janes JR, et al. Inhibition of
753 arginase by CB-1158 blocks myeloid cell-mediated immune suppression in the tumor
754 microenvironment. *J Immunother Cancer.* 2017;5(1):101.
755 26. Wei Y, Dong W, Jackson J, Ho TC, Le Saux CJ, Brumwell A, et al. Blocking LOXL2 and
756 TGFbeta1 signalling induces collagen I turnover in precision-cut lung slices derived from
757 patients with idiopathic pulmonary fibrosis. *Thorax.* 2021;76(7):729-32.
758 27. Jin S, Guerrero-Juarez CF, Zhang L, Chang I, Ramos R, Kuan CH, et al. Inference and analysis
759 of cell-cell communication using CellChat. *Nat Commun.* 2021;12(1):1088.
760 28. Roofeh D, Lin CJF, Goldin J, Kim GH, Furst DE, Denton CP, et al. Tocilizumab Prevents
761 Progression of Early Systemic Sclerosis-Associated Interstitial Lung Disease. *Arthritis*
762 *Rheumatol.* 2021;73(7):1301-10.

763 29. Group RC. Tocilizumab in patients admitted to hospital with COVID-19 (RECOVERY): a
764 randomised, controlled, open-label, platform trial. *Lancet.* 2021;397(10285):1637-45.
765 30. Khanna D, Lin CJF, Furst DE, Goldin J, Kim G, Kuwana M, et al. Tocilizumab in systemic
766 sclerosis: a randomised, double-blind, placebo-controlled, phase 3 trial. *Lancet Respir Med.*
767 2020;8(10):963-74.
768 31. Narvaez J, J LL, Alegre Sancho JJ, Molina-Molina M, Nolla JM, and Castellvi I. Effectiveness
769 and safety of tocilizumab for the treatment of refractory systemic sclerosis associated interstitial
770 lung disease: a case series. *Ann Rheum Dis.* 2019;78(11):e123.
771 32. Salcher S, Sturm G, Horvath L, Untergasser G, Kuempers C, Fotakis G, et al. High-resolution
772 single-cell atlas reveals diversity and plasticity of tissue-resident neutrophils in non-small cell
773 lung cancer. *Cancer Cell.* 2022;40(12):1503-20 e8.
774 33. Idzko M, Ferrari D, and Eltzschig HK. Nucleotide signalling during inflammation. *Nature.*
775 2014;509(7500):310-7.
776 34. Trang T, Beggs S, Wan X, and Salter MW. P2X4-receptor-mediated synthesis and release of
777 brain-derived neurotrophic factor in microglia is dependent on calcium and p38-mitogen-
778 activated protein kinase activation. *J Neurosci.* 2009;29(11):3518-28.
779 35. Le Guilcher C, Garcin I, Dellis O, Cauchois F, Tebbi A, Doignon I, et al. The P2X4 purinergic
780 receptor regulates hepatic myofibroblast activation during liver fibrogenesis. *J Hepatol.*
781 2018;69(3):644-53.
782 36. Werner S, Mesch S, Hillig RC, Ter Laak A, Klint J, Neagoe I, et al. Discovery and
783 Characterization of the Potent and Selective P2X4 Inhibitor N-[4-(3-Chlorophenoxy)-3-
784 sulfamoylphenyl]-2-phenylacetamide (BAY-1797) and Structure-Guided Amelioration of Its
785 CYP3A4 Induction Profile. *J Med Chem.* 2019;62(24):11194-217.
786 37. Summer R, Todd JL, Neely ML, Lobo LJ, Namen A, Newby LK, et al. Circulating metabolic
787 profile in idiopathic pulmonary fibrosis: data from the IPF-PRO Registry. *Respir Res.*
788 2024;25(1):58.

789 38. Lee JU, Song KS, Hong J, Shin H, Park E, Baek J, et al. Role of lung ornithine
790 aminotransferase in idiopathic pulmonary fibrosis: regulation of mitochondrial ROS generation
791 and TGF-beta1 activity. *Exp Mol Med.* 2024;56(2):478-90.
792 39. Pesce JT, Ramalingam TR, Mentink-Kane MM, Wilson MS, El Kasmi KC, Smith AM, et al.
793 Arginase-1-expressing macrophages suppress Th2 cytokine-driven inflammation and fibrosis.
794 *PLoS Pathog.* 2009;5(4):e1000371.
795 40. Raghu G, Richeldi L, Crestani B, Wung P, Bejuit R, Esperet C, et al. SAR156597 in idiopathic
796 pulmonary fibrosis: a phase 2 placebo-controlled study (DRI11772). *Eur Respir J.* 2018;52(6).
797 41. Wilson MS, Madala SK, Ramalingam TR, Gochuico BR, Rosas IO, Cheever AW, et al.
798 Bleomycin and IL-1beta-mediated pulmonary fibrosis is IL-17A dependent. *J Exp Med.*
799 2010;207(3):535-52.
800 42. Ruscitti C, Abinet J, Marechal P, Meunier M, de Meeus C, Vanneste D, et al. Recruited atypical
801 Ly6G(+) macrophages license alveolar regeneration after lung injury. *Sci Immunol.*
802 2024;9(98):eado1227.
803 43. Czystowska-Kuzmicz M, Sosnowska A, Nowis D, Ramji K, Szajnik M, Chlebowska-Tuz J, et al.
804 Small extracellular vesicles containing arginase-1 suppress T-cell responses and promote tumor
805 growth in ovarian carcinoma. *Nat Commun.* 2019;10(1):3000.
806 44. Zhang H, Liu J, Qu D, Wang L, Wong CM, Lau CW, et al. Serum exosomes mediate delivery of
807 arginase 1 as a novel mechanism for endothelial dysfunction in diabetes. *Proc Natl Acad Sci U*
808 *S A.* 2018;115(29):E6927-E36.
809 45. Roque W, and Romero F. Cellular metabolomics of pulmonary fibrosis, from amino acids to
810 lipids. *Am J Physiol Cell Physiol.* 2021;320(5):C689-C95.
811 46. Foo SS, Turner CJ, Adams S, Compagni A, Aubyn D, Kogata N, et al. Ephrin-B2 controls cell
812 motility and adhesion during blood-vessel-wall assembly. *Cell.* 2006;124(1):161-73.
813 47. Clausen BE, Burkhardt C, Reith W, Renkawitz R, and Forster I. Conditional gene targeting in
814 macrophages and granulocytes using LysMcre mice. *Transgenic Res.* 1999;8(4):265-77.

815 48. Ozaki T, Muramatsu R, Sasai M, Yamamoto M, Kubota Y, Fujinaka T, et al. The P2X4 receptor
816 is required for neuroprotection via ischemic preconditioning. *Sci Rep.* 2016;6:25893.
817 49. El Kasmi KC, Qualls JE, Pesce JT, Smith AM, Thompson RW, Henao-Tamayo M, et al. Toll-like
818 receptor-induced arginase 1 in macrophages thwarts effective immunity against intracellular
819 pathogens. *Nat Immunol.* 2008;9(12):1399-406.
820 50. Yata Y, Scanga A, Gillan A, Yang L, Reif S, Breindl M, et al. DNase I-hypersensitive sites
821 enhance alpha1(I) collagen gene expression in hepatic stellate cells. *Hepatology.*
822 2003;37(2):267-76.
823 51. Schneider C, Lee J, Koga S, Ricardo-Gonzalez RR, Nussbaum JC, Smith LK, et al. Tissue-
824 Resident Group 2 Innate Lymphoid Cells Differentiate by Layered Ontogeny and In Situ
825 Perinatal Priming. *Immunity.* 2019;50(6):1425-38 e5.
826 52. Reese TA, Liang HE, Tager AM, Luster AD, Van Rooijen N, Voehringer D, et al. Chitin induces
827 accumulation in tissue of innate immune cells associated with allergy. *Nature.*
828 2007;447(7140):92-6.
829 53. Kopf M, Baumann H, Freer G, Freudenberg M, Lamers M, Kishimoto T, et al. Impaired immune
830 and acute-phase responses in interleukin-6-deficient mice. *Nature.* 1994;368(6469):339-42.
831 54. Caudrillier A, Kessenbrock K, Gilliss BM, Nguyen JX, Marques MB, Monestier M, et al. Platelets
832 induce neutrophil extracellular traps in transfusion-related acute lung injury. *J Clin Invest.*
833 2012;122(7):2661-71.
834 55. Hao Y, Hao S, Andersen-Nissen E, Mauck WM, 3rd, Zheng S, Butler A, et al. Integrated
835 analysis of multimodal single-cell data. *Cell.* 2021;184(13):3573-87 e29.
836 56. McGinnis CS, Murrow LM, and Gartner ZJ. DoubletFinder: Doublet Detection in Single-Cell
837 RNA Sequencing Data Using Artificial Nearest Neighbors. *Cell Syst.* 2019;8(4):329-37 e4.
838 57. Heng TS, Painter MW, and Immunological Genome Project C. The Immunological Genome
839 Project: networks of gene expression in immune cells. *Nat Immunol.* 2008;9(10):1091-4.
840 58. Chen EY, Tan CM, Kou Y, Duan Q, Wang Z, Meirelles GV, et al. Enrichr: interactive and
841 collaborative HTML5 gene list enrichment analysis tool. *BMC Bioinformatics.* 2013;14:128.

842 59. Gene Ontology C, Aleksander SA, Balhoff J, Carbon S, Cherry JM, Drabkin HJ, et al. The Gene
843 Ontology knowledgebase in 2023. *Genetics.* 2023;224(1).
844 60. Kramer A, Green J, Pollard J, Jr., and Tugendreich S. Causal analysis approaches in Ingenuity
845 Pathway Analysis. *Bioinformatics.* 2014;30(4):523-30.
846 61. Palla G, Spitzer H, Klein M, Fischer D, Schaar AC, Kuemmerle LB, et al. Squidpy: a scalable
847 framework for spatial omics analysis. *Nat Methods.* 2022;19(2):171-8.
848 62. Satija R, Farrell JA, Gennert D, Schier AF, and Regev A. Spatial reconstruction of single-cell
849 gene expression data. *Nat Biotechnol.* 2015;33(5):495-502.
850

851 **Acknowledgements**

852 This work was supported by funding from the US Department of Defense (Grant W81XWH2110417 to
853 MB), the UCSF Bakar Aging Research Institute (Investigator Grant to MB), Longevity Impetus Grants
854 from Norn Group (MB and JGO), a UCSF Bakar Aging Research Institute investigator award (MB), the
855 Nina Ireland Program for Lung Health Innovative Grant Program (PY), and NIH (1R01HL142701-01 to
856 ABM and R01AI172754 SKP). The authors would like to acknowledge the staff within the Biological
857 Imaging Development CoLab (BIDC) at UCSF Parnassus Heights, particularly Kyle Marchuk and Austin
858 Edwards, for their support in microscopy experiments. Sequencing performed at the UCSF CAT was
859 supported by UCSF PBBR, RRP IMIA, and NIH 1S10OD028511-01. We are grateful to Dr. Clifford
860 Lowell for his valuable comments and suggestions on the manuscript. We thank Giovanni Palla and
861 Nathan Levy for help in extending the Squidpy package.
862

863 **Author contributions**

864 PY performed or assisted in all the experiments and in figure preparation. JGO performed single cell
865 sequencing experiments and analysis and figure preparation. KC and SP performed single cell library
866 preparation and sequencing, supervised by ARA. NB and AB assisted in functional experiments with
867 lung tissues and cells. PD assisted in human neutrophil isolation and coculture experiments under the
868 supervision of SKP. XY assisted PY in coculture experiments and microscopy under the supervision of

869 BL. JN performed flow cytometry of mouse lung cells supervised by ABM. KB, TJ, and JW performed
870 mouse breeding and development of crosses for experiments. TT and DS assisted in analysis of single
871 cell sequencing data from mouse lung fibroblasts. MM and HT provided deceased donor control lung
872 tissues supervised by MAM. LM, AG, CM, and VA performed Xenium spatial transcriptomic analysis
873 supervised by WE. CC and AW designed and implemented spatial proximity analysis of Xenium data.
874 RM generated and provided P2x4 floxed mice. WT and ST performed MIBI analysis under the guidance
875 of TB. PJW provided lung explants from IPF patients and helped to interpret associated imaging data.
876 KMT designed and performed metabolomic assays, assisted by PY. MB conceived of the work,
877 supervised experimental planning and execution, and wrote the manuscript with input from PJW and
878 KMT.
879

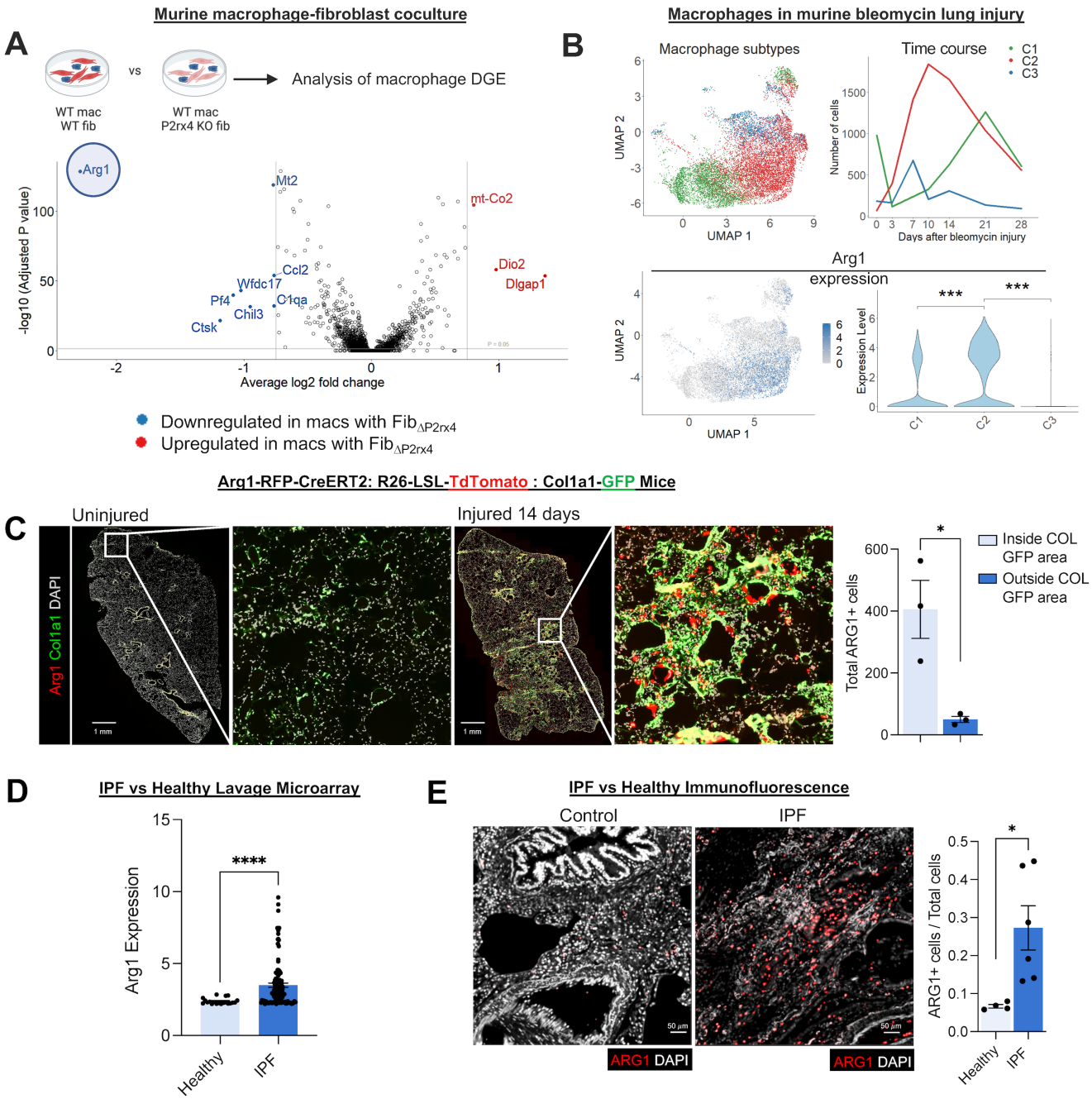

Figure 1: Arginase 1-expressing cells localize to the fibrotic niche in murine and human lung.

A) Volcano plot for macrophages from scRNAseq of macrophage-fibroblast cocultures for WT macrophages and fibroblasts versus WT macrophages cocultured with P2rx4 KO (*Pdgfrb-Cre: P2rx4 f/f*) fibroblasts. Significance was determined by Wilcoxon Rank Sum test corrected for multiple comparisons by Bonferroni method. Color-labeled genes had $p<0.05$ and absolute value of log2 fold change >0.75. Data represent n=2 separate cocultures.

B) Analysis of macrophages from bleomycin lung injury (data reanalyzed from[7]). Top left: Annotation of macrophages from multiple time points, according to C1, C2, or C3 macrophage annotation (as described in (7): C1=alveolar macrophages; C2=transitional monocyte-derived macrophages; C3=monocyte derived macrophages). Top right: Proportions of C1, C2, and C3 across time. Bottom left: Feature plot of Arg1 expression. Bottom right: Violin plot of Arg1 expression according to cluster (C1, C2, and C3). ***$p<0.001$ by Student's t-test.

C) Immunofluorescence imaging of tamoxifen-induced Arg1-RFP-CreERT2: LSL-tdTomato-Col1a1-GFP mice at 14 days after bleomycin injury. Quantification shows total Arg1+ cells inside and outside contiguous Col1a1-GFP+ areas. *p<0.05 by Student's t-test. +/- SEM.
D) *ARG1* expression by microarray analysis of gene expression of BAL cells from healthy (20 patients) and IPF (112 patients) from GSE70867(12). ****p<0.0001 by Mann-Whitney test. +/- SEM.
E) Representative immunofluorescence of human healthy control and IPF lung sections (n=4 and n=6, respectively) for ARG1. The quantification shows the proportion of ARG1+ cells (i.e., ARG1+ / total DAPI count) for each sample. *p<0.05 by Student's t-test. +/- SEM.

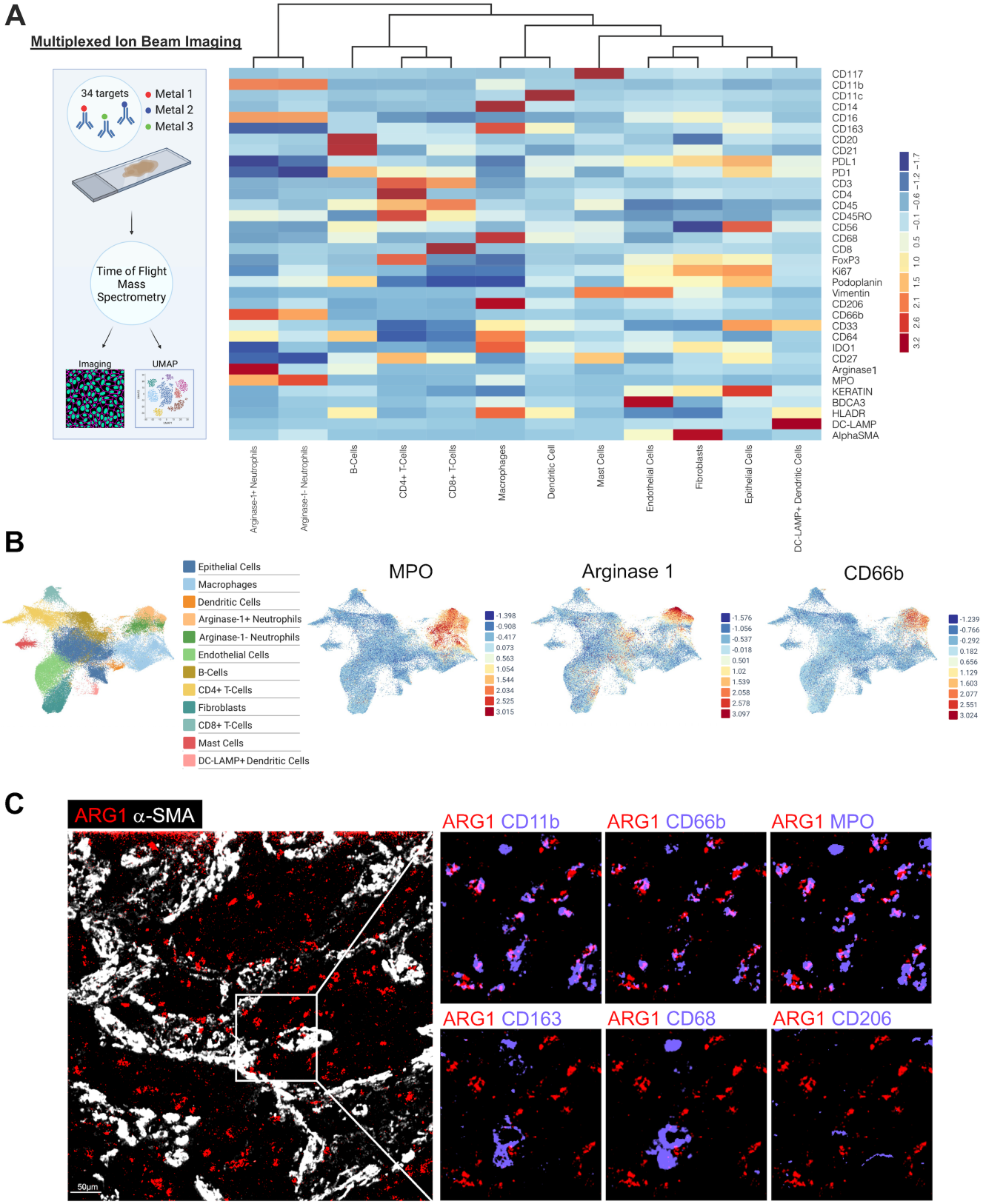

Figure 2: Arginase 1 is expressed predominantly by neutrophils in IPF.

A) Schematic of multiplexed ion beam imaging (MIBI) and heatmap of scaled marker expression from MIBI of sections from n=5 IPF explanted lungs.

B) MIBI UMAPs by cluster and individual markers.

910 C) MIBI images for individual markers within a representative field of view of IPF lung.
911

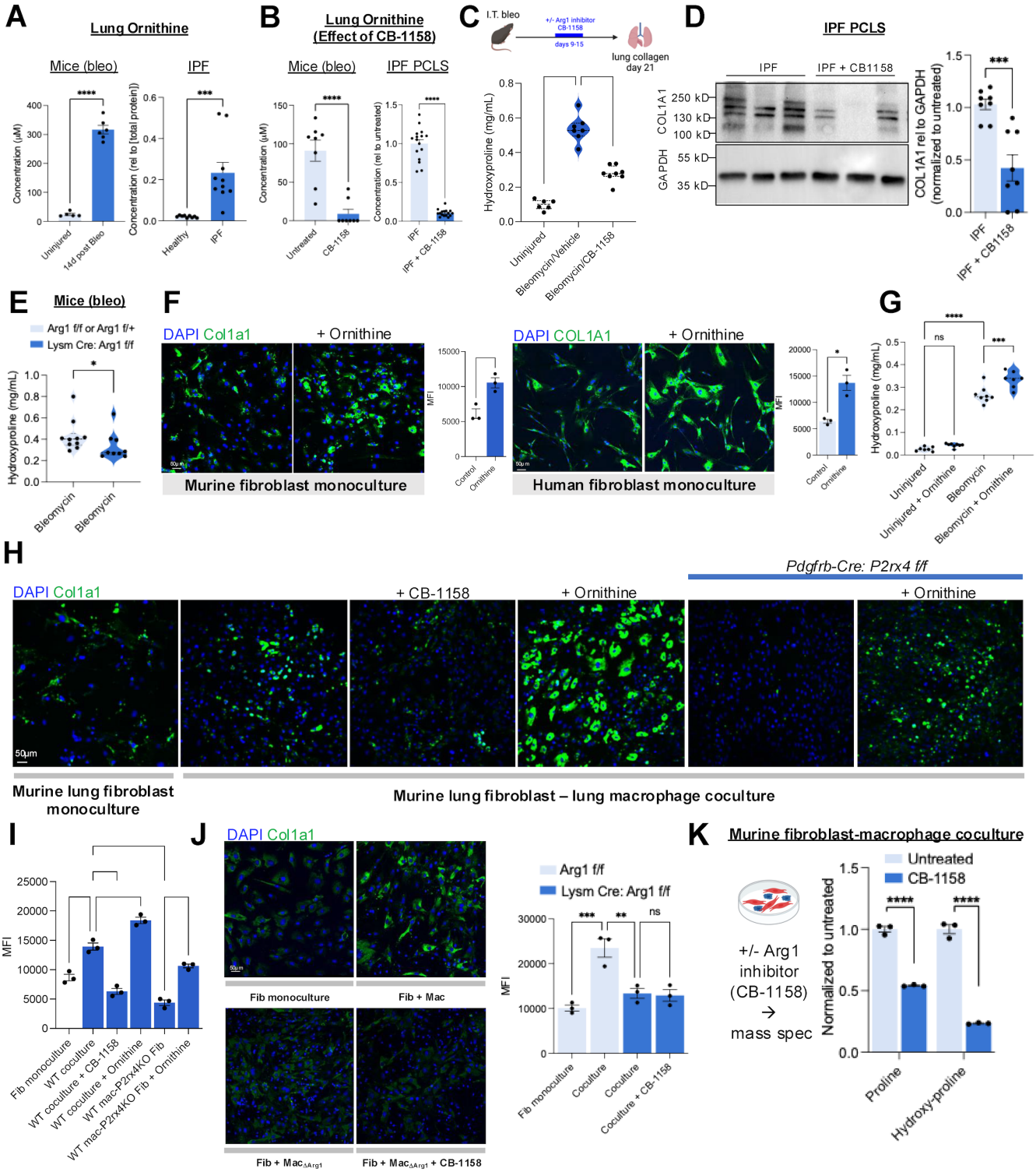

Figure 3: Arginase 1 regulates lung collagen via ornithine production.

A) Ornithine concentration measured in lysates of mouse lung (N=5 uninjured and N=6 injured mice), healthy human donor lung (N=9) and patient IPF lung explants (N=10). ****p<0.0001, ***p<0.001 by Student's t-test. +/- SEM.

B) Ornithine concentration with and without CB-1158 treatment of lungs of bleomycin-injured mice (N=8 in each condition) and cultured IPF PCLS (N=16 slices from a total of 3 patients). ****p<0.0001 by Student's t-test. +/- SEM.

C) Hydroxyproline assay for collagen content of lungs from injured and uninjured WT mice treated with or without Arg1 inhibitor CB-1158. Mice were dosed with 100 mg/kg of CB-1158 twice daily during days 9-15 post bleomycin. N=6, 7, 8 mice, left to right. ****p<0.0001 by 1-way ANOVA with post hoc Sidak's multiple comparisons tests. Median, upper, and lower quartiles indicated by dashed lines.

D) Representative immunoblot for COL1A1 from lysates of precision-cut IPF lung slices cultured for 24 hours with or without Arg1 inhibitor CB-1158. Quantitation is for slices from a total of n=3 patients. ***p<0.001 by Student's t-test. +/- SEM.

E) Hydroxyproline assay for collagen content of lungs from mice 21 days after bleomycin injury. N=10 and 9 mice, left to right. *p<0.05 by Mann-Whitney test. Median, upper, and lower quartiles indicated by dashed lines.

F) *Left:* Col1a1 immunofluorescence of monocultured mouse lung fibroblasts with or without ornithine treatment. Quantification is for n=3 separate cultures each. *p<0.05 by Student's t-test. *Right:* COL1A1 immunofluorescence of monocultured human lung fibroblasts with or without ornithine treatment. Quantification is for n=3 separate cultures each. *p<0.05 by Student's t-test. +/- SEM.

G) Hydroxyproline assay for collagen content of lungs from injured WT mice treated with or without ornithine (2 g/kg) twice daily by ornithine gavage during days 7 through 20. N=8, 7 mice, left to right. ***p<0.001, ****p<0.0001 by 1-way ANOVA with post hoc Sidak's multiple comparisons tests. Median, upper, and lower quartiles indicated by dashed lines.

H) Representative samples of Col1a1 immunofluorescence of mouse lung macrophage-fibroblast cocultures from WT or fibroblast-specific P2rx4 KO (Pdgfrb-Cre: P2rx4 f/f) mice treated with or without CB-1158 or ornithine.

I) Quantitation of Mean Fluorescence Intensity (MFI) from (H). N=3 biological replicates per condition. ****p<0.0001 by 1-way ANOVA with post hoc Sidak's multiple comparisons tests. +/- SEM.

J) Representative samples of Col1a1 immunofluorescence of mouse lung macrophage-fibroblast cocultures treated with or without CB-1158. "$Mac_{\Delta Arg1}$" indicates macrophages isolated from Lysm-Cre: Arg1 f/f mice, whereas "Mac" indicates Arg1 f/f controls. **p<0.01, ***p<0.0001 by 1-way ANOVA with post hoc Sidak's multiple comparisons tests. +/- SEM.

K) Relative quantities of proline and hydroxy-proline in lysates of murine primary lung fibroblasts isolated after coculture with macrophages, with or without CB-1158 inhibitor treatment, quantified by liquid chromatography-mass spectrometry. N=3 biological replicates for macrophages and fibroblasts, respectively. ****p<0.0001 by 1-way ANOVA with post hoc Sidak's multiple comparisons tests. +/- SEM.

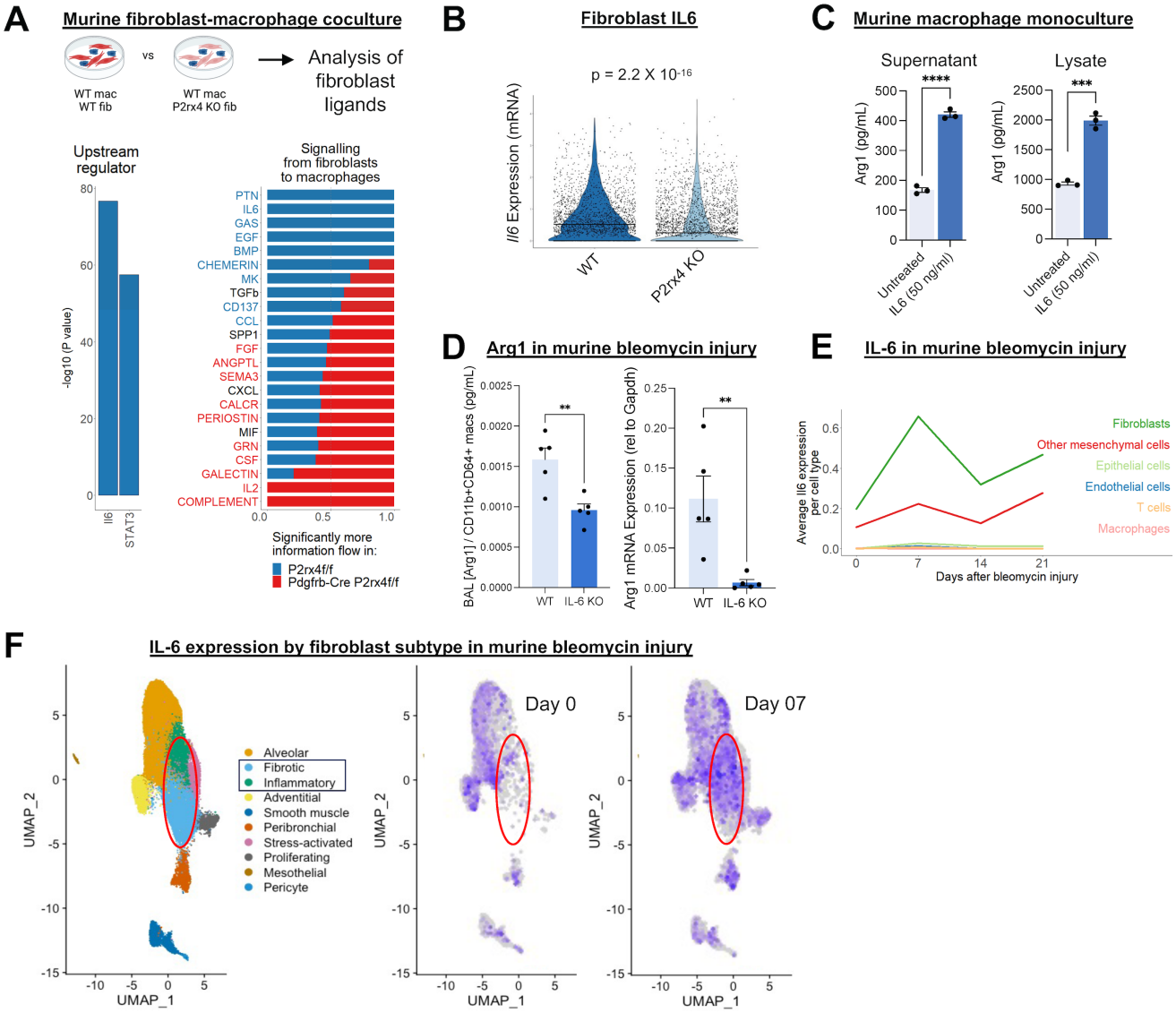

Figure 4: IL-6 is necessary for Arginase 1 expression after bleomycin injury in mice.

A) Left: Ingenuity Pathways Analysis of predicted upstream regulators for macrophages cultured with WT relative to P2rx4 KO fibroblasts. Right: CellChat plot comparing WT and P2rx4 conditions. Significance was determined by Wilcoxon test with $p<0.05$. Data represent n=2 separate cocultures.

B) Violin plot for IL-6 expression in WT relative to P2rx4 KO fibroblasts. Line shows median values. Data represent n=2 separate cocultures.

C) Arg1 ELISA of cell lysates and conditioned media collected from mouse lung macrophage monoculture 72 hours after IL-6 treatment. N=3 biological replicates per condition. ***$p<0.001$, ****$p<0.0001$ by Student's t-test. +/- SEM.

D) Left: Arg1 ELISA of bronchoalveolar lavage fluid normalized to lung CD11b+CD64+ macrophage count taken at day 14 from bleomycin-injured WT or IL6 KO mice. Right: Arg1 qPCR of CD11b+CD64+ macrophages. N=5 mice per condition. **$p<0.01$ by Student's t test. +/- SEM.

E) Quantification of *Il6* expression by cell type in cells sequenced by scRNAseq directly after isolation from the lung at steady state and multiple time points after injury (reanalysis of merged data(8, 9) normalized by Sctransform(62)).

F) UMAP of fibroblast subtypes (left) and IL-6 feature plots at steady state (center) and 7 days after bleomycin injury (right), from Tsukui et al.(8)

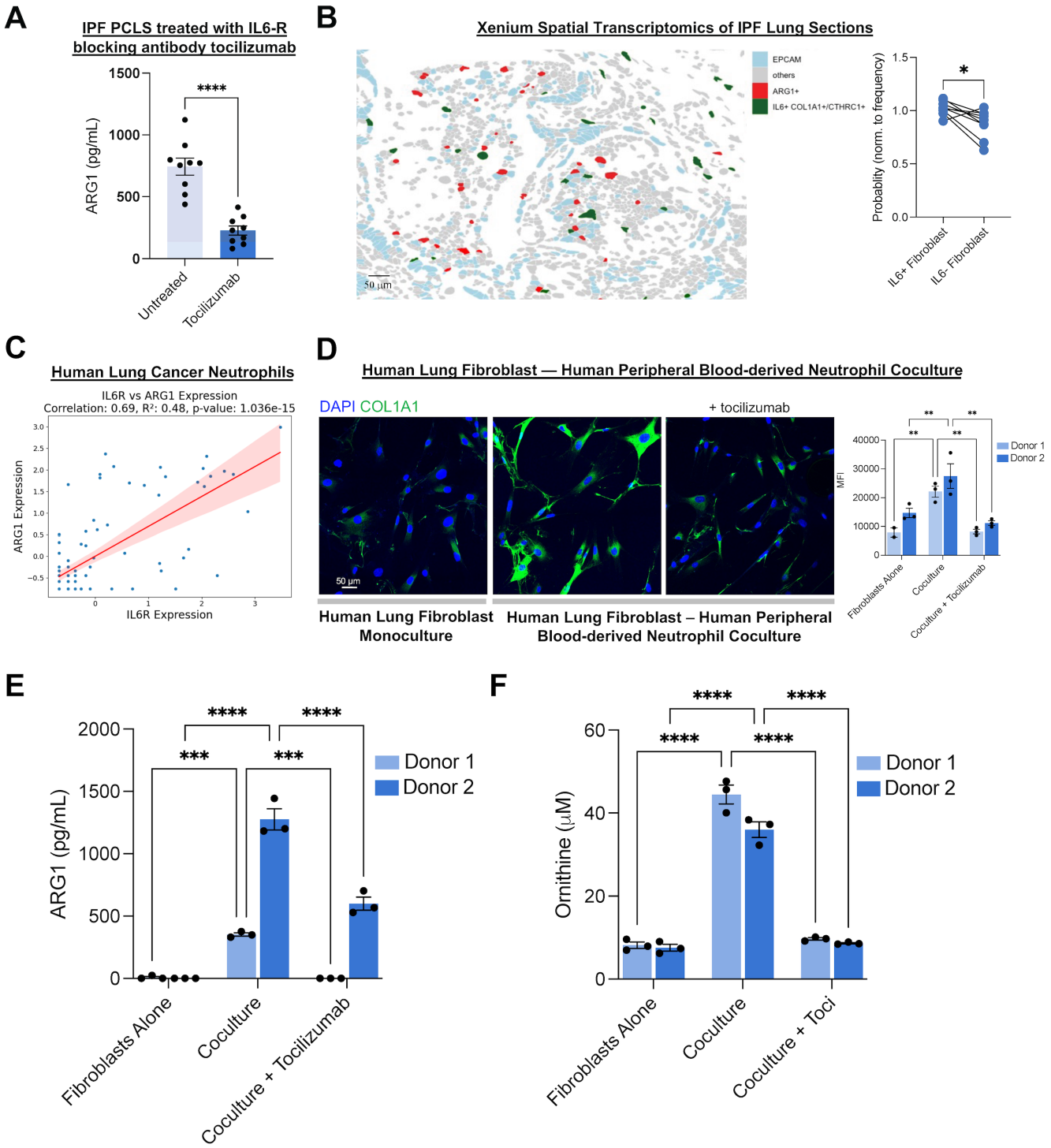

Figure 5: IL-6 is necessary for Arginase 1 expression in IPF lung and in cocultures of human blood-derived neutrophils and lung fibroblasts.

A) ARG1 ELISA of lysates of precision-cut IPF lung slices cultured for 24 hours with or without IL-6R blocking antibody tocilizumab. Data represent N=3 patients, with 3 slices per condition per patient assayed. ****p<0.0001 by Student's t-test. +/- SEM.

B) 10x Xenium spatial analysis: Left: Representative field of view showing cells expressing ARG1, EPCAM, and IL6+ fibroblasts (defined by co-expression of either COL1A1 or CTHRC1). Right: Proximity analysis of Xenium data: Data shown are for the probability ratio, P (exp | Arg1+)/P(exp), the probability of encountering an IL6+ fibroblast, normalized by fibroblast

990 frequency, at the radial distance of 25 μm from Arg1+ cells. *p<0.05 by paired Student's t-test.
991 Data are for N=9 separate patients. +/- SEM.
992 C) Correlation scatter plot of tissue-resident neutrophils expressing IL-6R and ARG1. Represents
993 integrated scRNAseq data of non-small cell lung cancer (NSCLC) from 19 datasets (32).
994 D) COL1A1 immunofluorescence of human lung fibroblasts that were either monocultured, or
995 cocultured with neutrophils with or without IL-6R blocking antibody (tocilizumab) treatment.
996 Quantification is for n=3 separate cultures each. Donor 1 and Donor 2 represent separate
997 donors for both neutrophils and fibroblasts.**p<0.01 by 2-way ANOVA followed by Sidak's
998 multiple comparisons test. +/- SEM.
999 E) ARG1 ELISA of conditioned media from cocultures of human blood-derived neutrophils and
1000 fibroblasts from healthy human explanted lung. ***p<0.001, ****p<0.0001 by 2-way ANOVA
1001 followed by Sidak's multiple comparisons test. +/- SEM.
1002 F) Ornithine concentration of conditioned media from the same cocultures as in (E). ****p<0.0001
1003 by 2-way ANOVA followed by Sidak's multiple comparisons test. +/- SEM.
1004

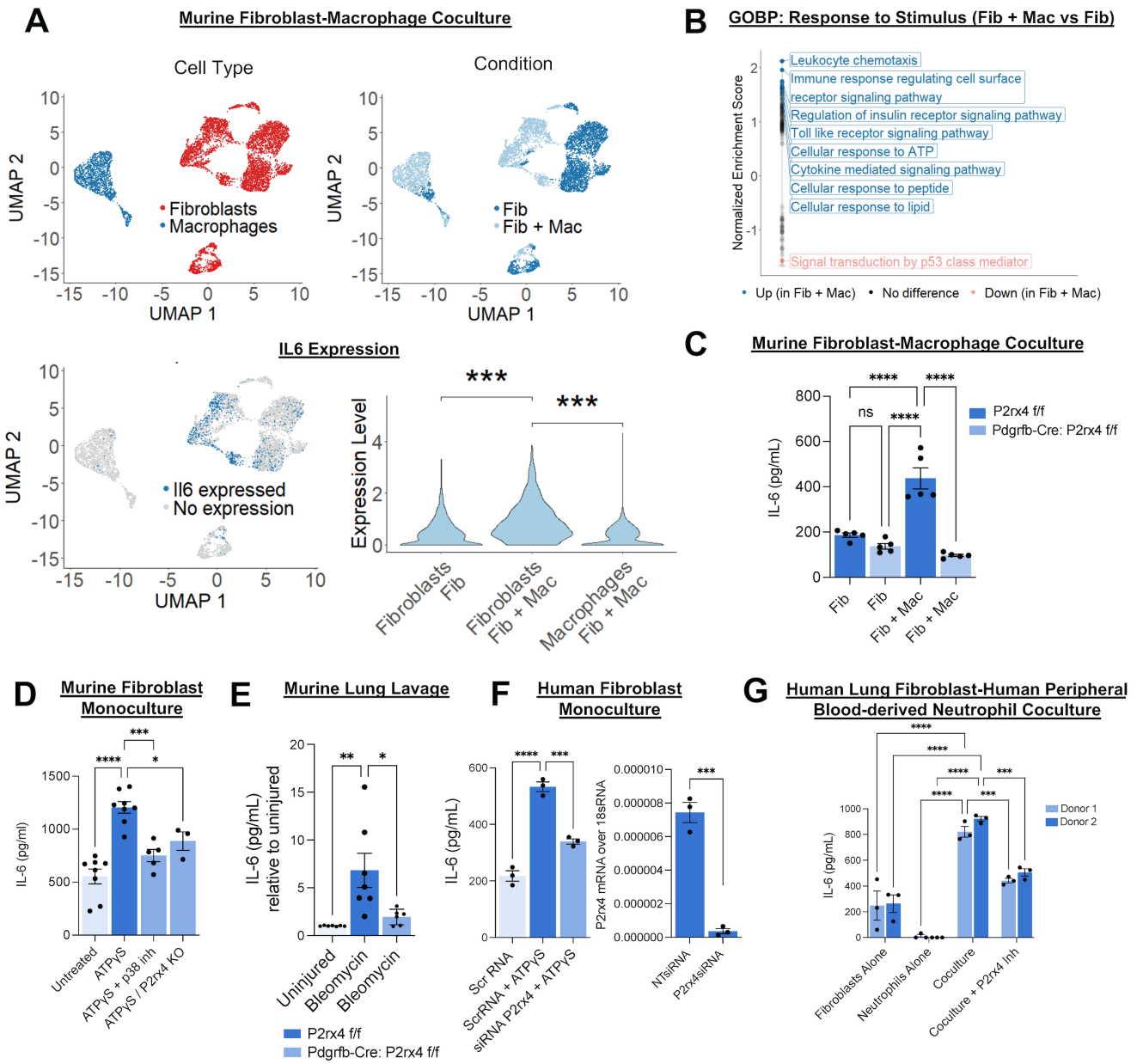

Figure 6: P2rx4 is necessary for IL-6 expression in mouse and human lung fibroblasts.

A) Top Left: UMAP plot of scRNAseq for macrophage-fibroblast cocultures with SingleR-based cell type annotation(2) shown. Data represent n=2 separate cultures for each condition. Top Right: UMAP plot for data showing sample of origin ("Fib" = fibroblast monoculture, "Fib + Mac" = fibroblast coculture with macrophages). Below Left: Feature plot showing *Il6* expression. Below Right: Violin plot of *Il6 expression*. ***p<0.001 by Wilcoxon Rank Sum test corrected for multiple comparisons by Bonferroni method.

B) Gene set enrichment analysis (GSEA) of fibroblast single cell transcriptomes in coculture with macrophages compared to fibroblast monoculture using GO "Response to stimulus" pathways.

C) IL-6 ELISA of conditioned media from macrophage-fibroblast cocultures with or without fibroblast-specific P2rx4 deletion. N=5 five biological replicates per condition. ****p<0.0001 by 1-way ANOVA with post hoc Sidak's multiple comparisons tests. +/- SEM.

D) IL-6 ELISA of conditioned media from monocultured mouse lung fibroblasts from WT mice, with and without ATPγS and SB203580 (p38 Map Kinase inhibitor) treatment or from fibroblast-specific P2rx4 KO (Pdgfrb-Cre: P2rx4 f/f) mice, with ATPγS treatment. N=8, 8, 5, 3 biological

1022 replicates per condition. *p<0.05, ***p<0.001, ****p<0.0001 by 1-way ANOVA with post hoc
1023 Sidak's multiple comparisons tests. +/- SEM.
1024 E) IL-6 ELISA from bronchoalveolar lavage from mice with or without fibroblast-specific P2rx4
1025 deletion. N=7, 7, 6 biological replicates, left to right. **p<0.01, *p<0.05 by 1-way ANOVA with
1026 post hoc Sidak's multiple comparisons tests. +/- SEM.
1027 F) IL-6 ELISA for conditioned media from human donor lung fibroblast monocultures with P2RX4
1028 siRNA KD or scrRNA, +/- ATPγS treatment (*left*, n=3 per condition. ***p<0.001, ****p<0.0001 by
1029 1-way ANOVA with post hoc Sidak's multiple comparisons tests; quantification of KD by qPCR
1030 on *right*, n=3 per condition, ***p<0.001 by Student's t-test). +/- SEM.
1031 G) IL-6 ELISA for conditioned media from human donor lung fibroblast monocultures, human blood
1032 derived neutrophil monocultures, or cocultures with or without P2RX4 inhibition with BAY-1797.
1033 Conditioned media were collected after 24 hours of culture. Each point re[presents a separate
1034 technical replicate. Neutrophils were derived from 2 separate blood donors, and fibroblasts were
1035 derived from 2 separate healthy lung donors. ***p<0.001, ****p<0.0001 by 2-way ANOVA
1036 followed by Sidak's multiple comparisons test. Donor 1 and Donor 2 represent separate donors
1037 for both neutrophils and fibroblasts. +/- SEM.